NUMERICAL MODELING OF WAVE DIFFRACTION IN ONE-DIMENSIONAL SHORELINE CHANGE MODEL

A THESIS SUBMITTED TO
THE GRADUATE SCHOOL OF NATURAL AND APPLIED SCIENCES
OF
MIDDLE EAST TECHNICAL UNIVERSITY

BY

CÜNEYT BAYKAL

IN PARTIAL FULFILLMENT OF THE REQUIREMENTS
FOR
THE DEGREE OF MASTER OF SCIENCE
IN
CIVIL ENGINEERING

DECEMBER 2006

Approval of the Graduate School of Natural and Applied Sciences

_____

Prof.Dr. Canan Özgen
Director

I certify that this thesis satisfies all the requirements as a thesis for the degree of Master of Science.

_____

Prof.Dr. Güney Özcebe
Head of Department

This is to certify that we have read this thesis and that in our opinion it is fully adequate, in scope and quality, as a thesis for the degree of Master of Science.

_____	_____
Assoc.Prof.Dr. Ahmet Cevdet Yalçıner Co-Supervisor	Prof.Dr. Ayşen Ergin Supervisor

Examining Committee Members

Assoc.Prof.Dr. İsmail Aydın (METU, CE) _____

Prof.Dr. Ayşen Ergin (METU, CE) _____

Assoc.Prof.Dr. Ahmet Cevdet Yalçıner (METU, CE) _____

Dr. Işıkhan Güler (METU, CE) _____

Engin Bilyay (M.S.) _____
(DLH, General Directorate of Railways,
Harbors and Airports Construction)

I hereby declare that all information in this document has been obtained and presented in accordance with academic rules and ethical conduct. I also declare that, as required by these rules and conduct, I have fully cited and referenced all material and results that are not original to this work.

Name, Last name: Cüneyt Baykal

Signature :

ABSTRACT

NUMERICAL MODELING OF WAVE DIFFRACTION IN
ONE-DIMENSIONAL SHORELINE CHANGE MODEL

Baykal, Cüneyt
M.S., Department of Civil Engineering
Supervisor: Prof.Dr. Ayşen Ergin
Co-Supervisor: Assoc.Prof.Dr. Ahmet Cevdet Yalçıner

December 2006, 95 pages

In this study, available coastal models are briefly discussed and under wind waves and a numerical shoreline change model for longshore sediment transport based on "one-line" theory is developed. In numerical model, wave diffraction phenomenon in one-dimensional modeling is extensively discussed and to represent the irregular wave diffraction in the sheltered zones of coastal structures a simpler approach based on the methodology introduced by Kamphuis (2000) is proposed. Furthermore, the numerical model results are compared with analytical solutions of accretion and erosion at a single groin. An application to a case study of a groin field constructed to the east side of Kızılırmak river mouth, at Bafra alluvial plain, is carried out by the numerical model. The results of comparisons show that the numerical model is in good agreement with the analytical solutions of shoreline changes at a groin. Similarly, numerical model results are compared with field data of Bafra and it is shown that they are in good agreement qualitatively. Therefore, the numerical model is accepted to be capable of representing of shoreline evolution qualitatively even for complex coastal regions.

Keywords: Longshore sediment transport, Shoreline change model, One-line theory, Wave diffraction, Analytical solutions

ÖZ

TEK BOYUTLU KIYI ÇİZGİSİ DEĞİŞİM MODELİNDE
DALGA SAPMASININ SAYISAL MODELLENMESİ

Baykal, Cüneyt
Yüksek Lisans, İnşaat Mühendisliği Bölümü
Tez Yöneticisi: Prof.Dr. Ayşen Ergin
Ortak Tez Yöneticisi: Doç.Dr. Ahmet Cevdet Yalçıner

Aralık 2006, 95 sayfa

Bu çalışmada, mevcut kıyı modelleri incelenmiş ve rüzgar dalgaları altında kıyı boyu katı madde taşınımına bağlı olarak "tek-çizgi" teorisine dayalı bir sayısal kıyı çizgisi değişim modeli geliştirilmiştir. Dalga sapmasının sayısal modellenmesi üzerine geliştirilen metodlar ayrıntılı bir şekilde incelenmiş ve Kamphuis (2000) tarafından düzensiz dalgaların sapma hesabı için verilen metoda dayalı daha basit bir yaklaşım modelde önerilmiştir. Geliştirilen sayısal model tek mahmuz için yığılma ve aşınma analitik çözümleri ile karşılaştırılmış ve Kızılırmak nehir ağzı, Bafra Delta'sında inşa edilmiş mahmuz sistemi için model uygulaması yapılmıştır. Geliştirilen model analitik çözümler ile nitelik ve nicelik olarak tutarlı olup saha ölçümleri ile de niteliksel olarak uyumlu bulunmuştur. Sayısal model kıyı çizgisi değişimini karmaşık kıyı alanlarında dahi niteliksel olarak gösterebilmektedir.

Anahtar Kelimeler: Kıyı çizgisi modeli, Tek-çizgi teorisi, Dalga sapması, Analitik çözümler

To My Family

ACKNOWLEDGEMENTS

I would like to express my sincere gratitudes to Prof.Dr. Ayşen Ergin, Assoc.Prof.Dr. Ahmet Cevdet Yalçıner and Dr. Işıkhan Güler for their supervision, support and valuable suggestions throughout this study. It has always been a privilege to work with them.

I would also like to thank Assoc.Prof.Dr. Mehmet Ali Kökpınar and Dr.Yakup Darama, from State Hydraulic Works (DSİ) for their assistance to test the numerical model with actual field data.

My very special thanks are attended to my dear friends Mr. Salih Serkan Artagan and Mr. Ilgar Şafak for their continuous support, help and patience throughout the whole study.

I would like to express my special thanks to my parents, for their encouragement, support and priceless affection at every stage of my life.

I extend my sincere thanks to the staff and technicians of Coastal and Harbor Engineering Laboratory for their kindness and cheerfulness at all times.

TABLE OF CONTENTS

LIST OF TABLES

TABLES

LIST OF FIGURES

FIGURES

LIST OF SYMBOLS

A	dimensionless parameter
A_p	sediment dependent scale parameter
B	beach berm height above still water level
C_{g0}	deep water wave group celerity
C_0	deep water wave celerity
C_K	empirical calibration factor
D_C	depth of closure
D_{LT}	limiting depth of longshore sediment transport
D_{50}	median grain size diameter
d	water depth
d_b	wave breaking depth
f	wave frequency
f_p	frequency at the spectral peak
g	gravitational acceleration
GB	alongshore distance away from the groin
GS	alongshore length of shadow zone on the breaker line
$(H_{1/3})_0$	the highest one-third deep water significant wave height
H_0	deep water significant wave height
H_b	breaking wave height
H_{bd}	modified wave breaking height
H_d	diffracted wave height in the lee of the breakwater
H_i	incident wave height at the tip of the breakwater
$H_{s,12}$	non-breaking significant wave height, that is exceeded 12 hr./year
H_{sa}	average deep water significant height
k	wave number
K	dimensionless empirical proportionality coefficient
K_d	coefficient of diffraction
l_{gb}	groin length from the seaward tip of groin to the breaking location
L	wave length

L_0	deep water wave length
L_b	breaking wave length
m_0	integral (zero moment) of the directional spectrum
m_b	beach slope at breaker location
p	in-place porosity
P_i	occurrence probability of wave with height H_i
$P_E(\theta)$	cumulative relative wave energy
Q	longshore sediment transport rate
	exceedence probability (: in Chapter 5)
Q_{net}	net longshore sediment transport rate
Q_0	amplitude of longshore sediment transport
r	radial distance from the breakwater tip to the point of interest
R_s	stability parameter
S_g	length of sheltered zone on the breaker line
S_{max}	spreading parameter
S_{max0}	deep water spreading parameter
SC	distance between the point of interest to the end of shadow zone on the breaker line
q	sources/sinks along the coast
t	time
T	significant wave period
U	wind speed
x	alongshore distance
X_g	spacing between the groins
W	dimensionless parameter
y	offshore distance
Y_g	groin length measured from inital shoreline
z	normal direction to x-y plane
α_0	deep water wave approach angle
α_b	breaking wave angle
α_{bd}	diffracted breaking wave angle

α_{bs}	breaking angle of wave from the end of the groin
α_{eb}	efficient breaking wave angle
α_i	incident wave angle at the tip of the structure
α_v	incident breaking wave angle at the groin
α_h	breaking wave angle in the illuminated region
β	angle between the breakwater alignment and radial
ε	diffusivity parameter
γ_b	wave breaker index
θ	shadow angle
ρ	water density
ρ_s	sediment density
Δt	time increment
Δx	alongshore grid spacing
Δy	offshore grid spacing
Δz	grid spacing along depth

LIST OF ABBREVIATION

1-D	One-Dimensional
2-D	Two-Dimensional
2-DH	Two-Dimensional Horizontal
2-DV	Two-Dimensional Vertical
3-D	Three-Dimensional
CEM	Coastal Engineering Manual
CERC	Coastal Engineering Research Center
DMİGM	General Directorate of Meteorological Affairs
DSİ	State Hydrualics Works
E	East
ENE	East-North-East
erf	Error Function
erfc	Complementary Error Function
ESE	East-South-East
GENESIS	Generalized Model for Simulating Shoreline Change
ierfc	First Integral of Complementary Error Function
i^2erfc	Second Integral of Complementary Error Function
N	North
NE	North-East
NLINE	N-Dimensional Contour Line Change Model
NNE	North-North-East
NNW	North-North-West
NW	North-West
ONELINE	One-Dimensional Shoreline Change Model
Q3-D	Quasi-Three-Dimensional
SPM	Shore Protection Manual
WNW	West-North-West

CHAPTER 1

INTRODUCTION

"It isn't the mountain ahead that wears you out
- it's the grain of sand in your shoe."
Robert Service

Coastal engineers and scientists have made numerous attempts to answer one simple and major question among a wide variety of challenging coastal problems for decades. Where will the shoreline be tomorrow? Next week? Next year? In a decade? Besides the complexity of coastal morphodynamics, local and temporal variations in the characteristics of coastal areas have made difficult for coastal engineers to answer this question. The available input data about the problem often is the main parameter in the determination of the methodology and limits the accuracy of the prediction of future changes in shoreline. Site specific features such as wave climate and storm history, bottom topography, sources of erosion and/or accretion, existing coastal structures and many other features and their single and combined effects on the reshaping of the shoreline should be taken into consideration for accurate modeling of the problem as much as possible.

Coastal problems and the necessity of implementation of integrated coastal zone management are mainly due to rapidly increasing use of coastal areas. In addition to the increasing development, the possible lack of control mechanisms and low-level of education of local people increase complexity of problems and severity of measures. The measures taken for the control of sediment budget in coastal areas are categorized in two groups as hard measures (jetties, groins, detached breakwaters, seawalls, dykes etc.) and soft measures (beacfills, sediment traps, etc.). Depending on the local characteristics and the short-term and long-term predictions of shoreline changes, these two types of measures may be applied as single or in combination.

The prediction of impacts of coastal defense measures is mainly based on documentation and monitoring of previously applied projects and application of predictive modeling tools. In addition to available analytical and empirical models, the continuous research for better understanding the physical processes responsible for shaping coastal morphology and the rapid advance in computer technology have initiated an increasing interest in developing powerful numerical models to simulate coastal processes and beach changes. Several categories of numerical models of beach evolution have been developed, ranging from simple 1-D models for idealized conditions to sophisticated 3-D models (Dabees, 2000). These numerical models are also available as powerful software packages for the purpose of engineering uses and research. Some well known of them are; GENESIS developed jointly by the Department of the Army (Waterways Experiment Station, Corps of Engineers, Vicksburg, MS, USA) and the Department of Water Resources Engineering (Lund Institute of Technology, University of Lund, Sweden); UNIBEST modules developed by WL, Delft Hydraulics (The Netherlands); and LITPACK developed by Danish Hydraulics Institute (Denmark).

As the physical processes in the coastal areas are simulated in more detail, the numerical models get complicated, which result in longer time in simulation, sensitivity analysis and model calibration and verification. Therefore, effectiveness of the model with respect to the problem should be discussed before simulation. Despite various limitations and assumptions, one-dimensional models have proven themselves to give at least qualitative results in the prediction of long-term shoreline changes. However, in order to achieve quantitative results with one-dimensional models also, the application site should agree with the limitations and assumptions of the "one-line" theory such as parallel bottom contours and equilibrium profile and the results should be calibrated with available field and laboratory measurements.

In this study, the development of a computer program based on previous works of shoreline change models, GENESIS (Hanson, 1987) and ONELINE (Dabees and Kamphuis, 1998), will be discussed. The program has been developed in the Middle

East Technical University, Civil Engineering Department, Coastal and Harbor Engineering Laboratory to investigate the impacts of several coastal measures to shoreline and nearshore wave transformation mechanisms in the vicinity of coastal structures (shoaling, breaking, refraction and diffraction). A comparison between conventional diffraction method (SPM; Shore Protection Manual, 1984) and other methods based on regression analysis of diffraction coefficient from Goda's diffraction diagrams for random waves (Goda, 1985) has been made. The shoreline changes at a groin have been compared with the analytical solutions (Pelnard-Considere, 1956).

In Chapter 2, an overview of coastal models is briefly discussed.

In Chapter 3, the theoretical background of the program developed, determination of the nearshore wave characteristics and comparison of available diffraction methods are presented.

In Chapter 4, analytical solutions for shoreline changes at a groin are introduced and the numerical model results are compared with analytical solutions.

In Chapter 5, the numerical model is applied to a case study and the model results are compared with actual field measurements.

In Chapter 6, discussion and conclusion are presented and future studies are recommended.

CHAPTER 2

LITERATURE REVIEW

Coastal areas are our common heritage. The planning and use of these areas without being aware of existing natural processes are often fatal. These processes are highly sophisticated dynamic events ranging from microscale physical phenomena, such as the movement of a particular sand grain, to macroscale phenomena such as the influence of the global mean sea level rise on beach change (Hanson, 1987). Sediment transport mechanisms, wave kinematics and interactions between waves and coastal structures and bottom topography are essential topics to understand beach changes. To investigate coastal processes and influences of human activities in coastal areas, numerous studies have been made for years and consecutively several types of models have been developed. In this chapter an overview of sediment models is presented.

2.1 OVERVIEW OF COASTAL SEDIMENT MODELS

A possible way of understanding the nature is to model and observe the parameters involved. Traditionally, models have been grouped into one of four categories; empirical, analytical, numerical or physical depending on the character and complexity of the equations involved and the solution technique. Empirical models are based on field observations or experimental data. Analytical solutions are derived from governing physical expressions. Both empirical and analytical solutions give quick results and are quite practical for computation of shoreline evolution and verification of studies. For detailed investigation of natural processes in coastal areas, physical or numerical (derived from analytical solutions) models are commonly implemented. In coastal engineering, physical models have been used for simulating topographical changes. Due to the fact that these models suffer from serious deficiencies, such as high costs and scaling problems, the use of

numerical models has increased in recent years. Numerical models possess certain advantages over physical models in allowing the testing of a wide range of parameters, adaptability to a variety of sites, economical operation, and the absence of scale effects (Hanson, 1987).

Coastal planners and managers are primarily concerned with time scales of years to decades, longshore length scales of 10's-100's of kilometers, and cross-shore length scales of 1-10's of kilometers. Within coastal zone management, prediction of coastal evolution with numerical models has proven to be a powerful technique to assist in the understanding of processes involved and, in the case of necessary interventions, selection of the most appropriate project design. Models provide a framework for organizing the collection and analysis of data and for evaluating alternative future scenarios of coastal evolution. In situations where engineering activities are involved, models are preferably used in developing problem formulation and solution statements, and, importantly, for efficiently evaluating alternative design and optimizing the selected design (Hanson et al., 2003).

The prediction of shoreline evolution can be simplified by separating the changes due to longshore processes, largely responsible for long-term changes and those caused by cross-shore processes tending to operate on much shorter time scales. A notable exception to this generalization is the shoreline change related to long-term sea-level variability which results in a readjustment of the profile to the new water levels and is a cross-shore response (Miller and Dean, 2004). Depending on the coastal processes and scope of the study, morphological models expand from simple one-dimensional to sophisticated 3-D models. The uses of numerical models for different spatial and temporal scales are given in Figure 2.1.

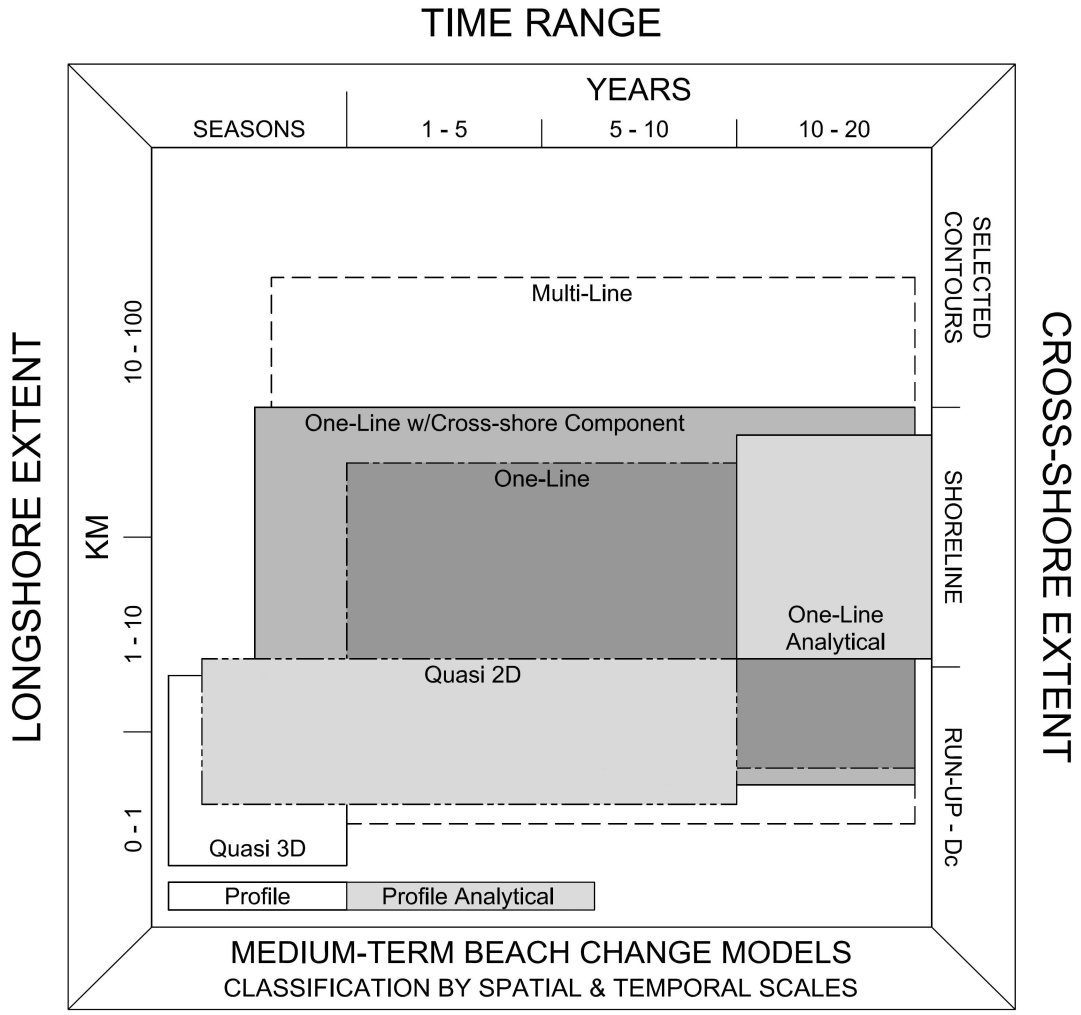

Figure 2.1 Classification of beach change models by spatial and temporal scales (Hanson et al., 2003)

As shown in Figure 2.1, the medium-term beach models are classified with respect to their longshore extent, time range and cross-shore extent. One-dimensional numerical models are preferable for most of the cases due to their applicability in wide ranged temporal (from 1 year up to 20 years) and spatial scales (from 0.5 kilometer up to 10 kilometers). Besides, seasonal changes of shorelines may be observed by one-dimensional models with a cross-shore module included. The applicability and success of one-dimensional models lead to development of multi-line models which extend the limits of applicability of one-dimensional models. Beach profile models are used to study short-term (from a storm duration or

seasonal changes up to 1 year) evolution of a beach profile. More complex models like quasi 3-D and quasi 2-D models are generally utilized for short- (up to 1 year) and medium-term (up to 10 years) shoreline changes respectively due to their complexity and intensive computations.

The available numerical models can be classified under three main categories; shoreline change models, beach profile models, and 3-D models (Dabees, 2000).

2.1.1 Shoreline Change Models

The fundamentals of shoreline change models were first established by Pelnard-Considere (1956), who set down the basic assumptions of the "one-line" theory, derived a mathematical model, and compared the solution of shoreline change at a groin with laboratory experiments. Bakker (1968) extended the concept to account for possible on–offshore transport and formulated a two-line schematization of the profile. Additional contributions to such models have been produced by LeMéhauté and Soldate (1978) for the inclusion of wave refraction and diffraction and by Fleming and Hunt (1976) for the bathymetry modification as a change in depths at a set of schematized grid points (Capobianco et al., 2002).

A common observation is that the beach profile maintains an average shape that is characteristic of the particular coast, apart from times of extreme change as produced by storms. For example, steep beaches remain steep and gently sloping beaches remain gentle in a comparative sense, in the long term. Although seasonal changes in wave climate cause the position of the shoreline to move shoreward and seaward in a cyclical manner, with corresponding change in shape and average slope of the profile, the deviation from an average beach slope over the total active profile is relatively small. If the profile shape does not change, any point on it is sufficient to specify the location of the entire profile with respect to a baseline. Thus, one contour line can be used to describe change in the beach plan shape and volume as the beach erodes and accretes. This contour line is conveniently taken as the readily observed shoreline, and a model of this process is therefore called a

"shoreline change" or "shoreline response" model. Sometimes the terminology "one-line" model, a shortening of the phrase "one contour line" model is used with reference to the single contour line. A second geometric assumption is that sand is transported alongshore between two well-defined limiting elevations on the profile. The shoreward limit is located at the top of the active berm, and the seaward limit is located where no significant depth changes occur, the so-called depth of (profile) closure. Restriction of profile movement between these two limits provides the simplest way to specify the perimeter of a beach cross-sectional area by which changes in volume, leading to shoreline change, can be computed (Capobianco et al., 2002).

The general approach to numerical models of shoreline change involves the division of the coastline into a large number of individual cells or compartments. Equations relating the alongshore sediment transport rate to the wave parameters and to velocities of alongshore currents are employed to calculate the shift of sand from one cell to another. The application of a continuity equation allows for the conversion of volumes of sand entering or exiting a particular cell into the resulting shoreline changes (Capobianco et al., 2002).

The "one-line" theory also assumes small angles of wave incidence. The analytical solutions provided a simple and quick approach for preliminary estimation of the shoreline response to various engineering activities. However, for thorough analysis and in situations involving complex boundary conditions, numerical modeling of beach change is essential (Dabees, 2000). One-dimensional shoreline evolution models have demonstrated their predictive capabilities in numerous projects (Hanson, 1987).

The "one-line" theory was first numerically implemented by Price, Tomlinson and Willis (1973), and followed by many others. Early numerical shoreline response models required extensive modification and special refinements for any particular study. The advance in computer technology aided the development of generalized shoreline change numerical models (Dabees, 2000). Examples of such general-

purpose models are GENESIS (Hanson, 1987) and ONELINE (Dabees and Kamphuis, 1998). A review of shoreline change models by Roelvink and Broker (1993) indicates necessary improvements and further studies for constituents such as long wave effects and details of wave current fields. On the other hand, simpler models that utilize empirical formulae derived from laboratory and field measurements may provide similar or even more realistic results using standard data available in most engineering applications (Dabees, 2000).

2.1.2 Beach Profile Models

Beach profile models are utilized for simulating short-term profile evolutions mainly caused by cross-shore movement of sediment particles (Dabees, 2000). The structure of such models is similar to that described for shoreline change models, i.e., a dynamic or transport equation that prescribes the sediment flow across the profile, and a continuity equation that integrates the differences between sediment flows in and out of a computational cell and equates those differences to changes in profile elevation. Several models have developed based on breaking waves as the cause of changes in profile (Dally and Dean, 1984; Kriebel And Dean, 1984; Larson and Kraus, 1989). Deterministic cross-shore models calculate wave transformation and the time averaged velocities across the profile. The sediment transport is then calculated as a function of the horizontal velocities and local bottom conditions using Bailard's (1981) energetics approach. Such models are UNIBEST-TC (Stive & Battjes, 1984; Roelvink et al, 1995) and LITCROSS (Broker-Hedegaard et al., 1991) (Dabees, 2000).

These models have been extensively used to evaluate the immediate response to storm conditions and to evaluate the initial response phase of a fill, but only limited effort have been devoted to the recovery phase following storms. Zheng and Dean (1997) have published an intercomparison of four ‘‘erosion models’’ based on large scale wave tank experiments. The overall message is that a number of relatively reliable tools are now available to handle erosional situations, but much more difficult is handling accretional situations. This is a problem while moving from the

examination of the response to single storms or stormy seasons to the examination of long-term evolution (resulting from sequences of erosional and accretional phases of variable duration) (Capobianco et al., 2002).

This type of models has been quite successful in predicting short-term events, however, applications for medium- and long-term predictions have been limited because of difficulties in formulating sediment transport formulas that produce reliable and robust profile evolution at these time scales (Hanson et al., 2003). On the other hand, profile models have been highly useful as a modeling tool to describe very long-term profile evolution, for example to simulate response to sea level rise or barrier island formation and movement (Cowell et al., 1994). The very long term profile models rely on transport formulas that are based on some sort of equilibrium. Thus, it seems reasonable to assume that satisfactory modeling results at medium- and long-term scales could also be achieved through formulations that rely on equilibrium concepts (Hanson et al., 2003).

The complexity involved in modeling the extremely dynamic nearshore region has led to the development of a number of different approaches. Roelvink and Broker (1993) and Van Rijn et al. (2003) provide valuable reviews and intercomparisons of many of the state-of the-art European cross-shore profile models. Roelvink and Broker (1993) classified the different modeling techniques into four categories: descriptive models (e.g., Wright and Short, 1984), equilibrium profile models (e.g., Swart, 1975), empirical profile evolution models (e.g., Larson and Kraus, 1989) and process-based models (e.g., Dally and Dean, 1984). Davies et al. (2002) further divided the process-based models into two categories: research models, containing full, detailed descriptions of the governing physics, and practical models that simplify the governing processes to varying degrees and which are more empirical in nature (Miller and Dean, 2004).

2.1.3 3-D Beach Evolution Models

The aperiodic nature of storm events, the uncertainty of future weather conditions and complex coastal morphologies have forced scientists to research more sophisticated models. As a result of these studies highly detailed process based morphological models exist today. However, these models tend to be computationally intensive and their accuracy near the shoreline over a broad spectrum of relevant time scales has not been fully demonstrated yet. Additionally, the complexity and computational costs involved in applying these detailed models to the nearshore region, over long time scales, makes them inefficient at the present time for long-term shoreline studies (Miller and Dean, 2004).

Larson, Kraus and Hanson (1990) presented a schematized 3-D model by joint use of the shoreline change model GENESIS and the profile change model SBEACH (Larson and Kraus, 1989). Uda et al., (1996) developed a contour line change model for coasts with steep slopes. Uda's model still makes the fundamental assumption of small incident wave angles. The model was used to simulate beach evolution behind breakwaters and to model the development of a river mouth delta (Uda et al., 1998). These contour line models can be viewed as a group of one-dimensional models linked by cross-shore interchange of sediment between them. The cross-shore transport is calculated based on the difference between the existing profile shape changes such as the formation of beach berms and nearshore bars (Dabees, 2000). Another contour line model, NLINE, that simulates long-term 3-D morphology changes for complex beach/structure configurations and allows the local profile formation of bars and berms is developed by Dabees and Kamphuis (1999; 2000).

In fully three-dimensional (3-D) models, the hydrodynamics equations are written in three dimensions. Finite difference models, for example, schematize the domain over a 3-D grid, as shown in Figure 2.2.

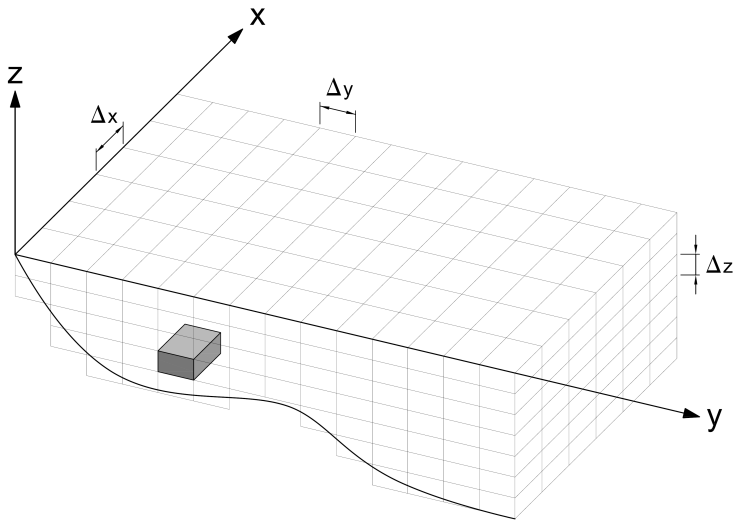

Figure 2.2 Three-dimensional (3-D) modeling (Kamphuis, 2000)

A complete 3-D representation requires longer computer time and memory yet still some fully 3-D models have been successfully developed. Three-dimensional models can be simplified into two-dimensional (2-D) models. Using vertically integrated values for the fluid flow, results in a 2-D model with a horizontal computational grid (2-DH model), shown in Figure 2.3. This type of models can be applied to solve medium-term transport problems (Kamphuis, 2000).

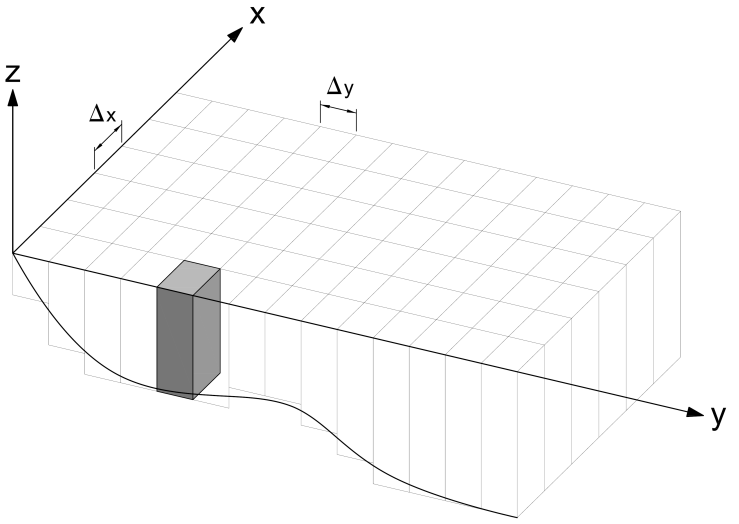

Figure 2.3 Two-dimensional (2-DH) modeling (Kamphuis, 2000)

A simplification of the 3-D model can be achieved by ignoring all alongshore variations in water levels, fluid velocities and their derivatives. This results in a cross-shore model (2-DV model) calculated over a 2-D vertical grid, shown in Figure 2.4. These models are essentially short-term models (Kamphuis, 2000).

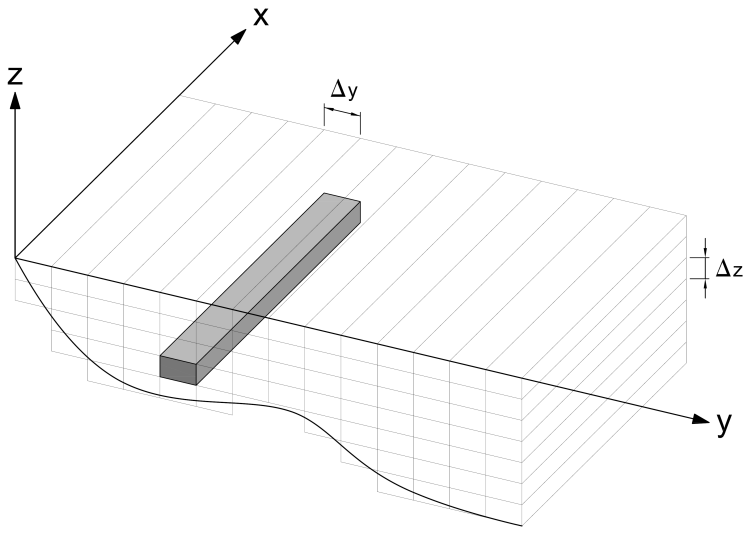

Figure 2.4 Two-dimensional (2-DV) modeling (Kamphuis, 2000)

Combining the two concepts in 2-D modeling, 2-DH and 2-DV, quasi-three-dimensional models (Q3-D) have been developed. This type of models are computationally extensive and requires detailed data for model verification. Recently, promising results are being acquired by quasi-3D models which operate on the dynamic scale of long-wave energy variations (Reniers et al., 2001). Examples of such models are LITPACK (Danish Hydraulics Institute), 3D-SHORE (Shimizu et al., 1996), and TELEMAC (Pechon and Teisson, 1996). De Vriend et al. (1993) referred to this class of models as medium-term coastal area models as their temporal scales vary from 1 to 5 years.

In this study, the numerical model developed is based on previous studies of one-dimensional shoreline change models: GENESIS (Hanson, 1987) and ONELINE (Dabees and Kamphuis, 1998). A one-dimensional model approach is preferred due to the facts that this type of models have wide ranged applicabilities in temporal and

spatial scales, requires less detailed input data and computer time and may give both qualitatively and quantitatively acceptable results which may be used for both engineering and scientific purposes.

CHAPTER 3

ONE-DIMENSIONAL NUMERICAL MODELLING

In this chapter, the development of a shoreline evolution model based on "one-line" theory in the Middle East Technical University, Civil Engineering Department, Coastal and Harbor Engineering Laboratory is given.

The topics that are discussed in detail include the investigation of developed methodologies representing sea bottom effect on waves and interactions between waves and coastal structures (i.e. groins and jetties).

3.1 ONE-LINE THEORY

"One-line" theory was first introduced by Pelnard-Considere (1956). In his study, the shoreline change at a groin was expressed by closed-form mathematical solutions for certain idealized cases and the results were verified with laboratory experiments. Afterwards, these mathematical equations set up the framework of numerical shoreline evolution models. The fundamental assumption of the theory is the concept of "equilibrium beach profile", that cross-shore transport effects such as storm-induced erosion and cyclical movement of shoreline position associated with seasonal changes in wave climate are assumed to cancel over a long simulation period and the migration of shoreline position in time is due to longshore sediment transport only. Although equilibrium beach profile assumption is verified by numerous observations, in cases such that excessive erosion happens in front of a seawall, bottom slope changes and equilibrium profile vanishes along the seawall (Hanson and Kraus, 1986). Another important assumption is that the longshore sediment transport is limited over an active depth from berm height at the shore side to a certain depth called as "depth of closure" at the sea side (Capobianco et al., 2002).

3.2 EQUILIBRIUM BEACH PROFILE

The existence of an equilibrium beach profile (sometimes called equilibrium beach profile) is a basic assumption of many conceptual and numerical coastal models. Dean (1990) listed characteristic features of profiles as follows:

- Profiles tend to be concave upwards.
- Fine sand is associated with mild slopes and coarse sand with steep slopes.
- The beach (above the surf zone) is approximately planar.
- Steep waves result in milder inshore slopes and a tendency for bar formation.

Based on studies of beaches in many environments, Bruun (1954) and Dean (1976, 1977) have shown that many ocean beach profiles exhibit a concave shape such that the depth varies as the two-thirds power of distance offshore along the submerged portions as given in equation (3.1);

$$d = A_p \cdot y^{2/3} \tag{3.1}$$

where d is the water depth at distance y from the shoreline and A_p is the profile shape parameter which can be calculated from sediment characteristics (particle size or fall velocity) alone (see Figure 3.1).

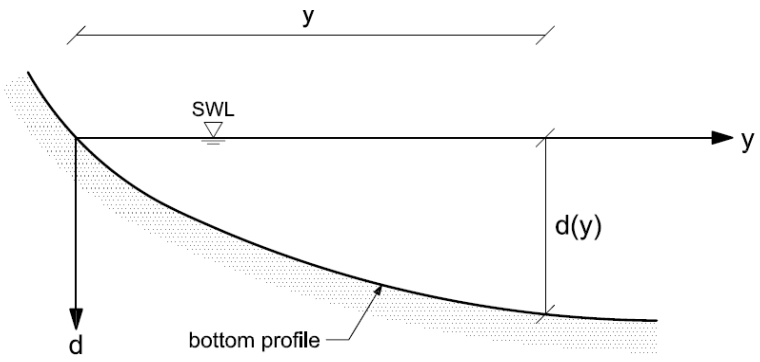

Figure 3.1 Beach profile shape (Dean's Profile)

Moore (1982) and Dean (1983) graphically relate the profile shape parameter (A_p) to the median grain size (D_{50}). Kamphuis (2000) redefines this graphical relationship with an exponential relationship given as

$$A_p = [1.04 + 0.086 \cdot \ln(D_{50})]^2 \quad \text{for} \quad 0.0001 \le D_{50} \le 0.001 \text{ meters} \qquad (3.2)$$

In the model, an equilibrium beach profile defined above has been used to represent the actual sea bottom profile.

3.3 GOVERNING EQUATIONS

Following the assumptions of "one-line" theory, a mathematical model for long-term shoreline evolution can be described by a conservation of mass equation (3.3) and an equation of sediment transport for a sandy beach system (3.5) or (3.6).

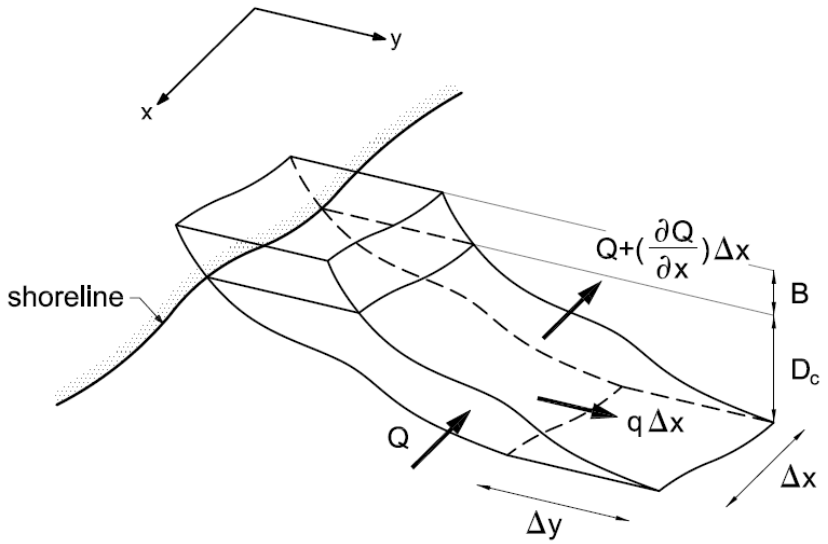

Figure 3.2 Definition sketch for conservation of mass for a sandy beach system

As the principle of mass conservation applies to the system at all times, the following differential equation is obtained,

$$\frac{\partial y}{\partial t} = -\frac{1}{(D_c + B)} \cdot \left(\frac{\partial Q}{\partial x} + q \right) \tag{3.3}$$

where y is the shoreline position, x is the longshore coordinate, t is the time, Q is the longshore sand transport, q represents sand sources or losses along the coast (such as river discharges, beach nourishment or net cross-shore sand loss), D_c is the depth of closure and B is the berm height. The depth of closure can be calculated from equation (3.4) presented by Hallermeier (1978) where $H_{s,12}$ and T are the significant wave height exceeded 12 hours per year and associated period respectively.

$$D_C = 2.28 \cdot H_{s,12} - 68.5 \cdot \left(\frac{H_{s,12}^2}{gT^2}\right) \tag{3.4}$$

For the calculation of longshore sediment transport rate, several mathematical expressions are available. Examples of such expressions are the CERC formula (3.5) (SPM, 1984), and the Kamphuis (1991) formula (3.6).

$$Q = \frac{K}{16 \cdot (\rho_s / \rho - 1) \cdot (1 - p)} \cdot \sqrt{\frac{g}{\gamma_b}} \cdot H_b^{5/2} \cdot \sin(2\alpha_b) \quad (\mathrm{m^3/sec}) \tag{3.5}$$

Q is the volume of sediment moving alongshore per unit time, K is the dimensionless empirical proportionality coefficient presented by SPM (1984) as $K_{SPM\ sig}$ = 0.39 based on computations utilizing the significant wave height. ρ_s is sediment density taken as 2,650 kg/m^3 for quartz-density sand and ρ is the water density (1,025 kg/m^3 for 33 parts per thousand (ppt) salt water and 1,000 kg/m^3 for fresh water). g is the gravitational acceleration (9.81 m/sec^2); and p is the in-place sediment porosity taken as 0.4. The breaker index (γ_b) is taken as 0.78 for flat beaches and increases to more than 1.0 depending on beach slope (Weggel, 1972). H_b and α_b are the significant breaking wave height and breaking wave angle respectively.

$$Q = 7.3 \cdot C_K \cdot H_b^2 \cdot T^{3/2} \cdot m_b^{3/4} \cdot D_{50}^{-1/4} \cdot \sin^{3/5}(2\alpha_b) \quad (\text{m}^3/\text{hrs}) \tag{3.6}$$

In the Kamphuis (1991) formula, the effect of significant wave period (T), median particle size in surf zone (D_{50}) and the beach slope (m_b) at the depth of breaking found from equation (3.7) and the distance from still water beach line to the breaker line are taken into consideration in addition to the significant breaking wave height and breaking wave angle. The in-place sediment porosity is taken as 0.32. C_K is used as an empirical calibration factor.

$$m_b = \frac{2}{3} \cdot A_p^{3/2} \cdot d_b^{-1/2} \tag{3.7}$$

Both CERC and Kamphuis longshore transport formulas are utilized in shoreline evolution models extensively. Although these expressions have been verified by several researches for years, their predictive capabilities are affected by numerous parameters. Because it is a very difficult task to represent the whole longshore transport mechanism with one simple expression. The determination of the type of expression to be utilized depends on the user as well as the climate data available. It has been seen that the Kamphuis (1991) formula produces more consistent predictions than the CERC formula for both spilling and plunging breaking wave conditions due to inclusion of wave period in the expression, which has significant influence on the breaker type. However, it seems most appropriate to use the CERC formula for storm events and the Kamphuis (1991) formula for low-energy events (less than 1 m in wave height) (Wang et al., 2002). Another advantage of using the CERC expression is that it takes into consideration the density of the sediment grains which may vary for beaches composed of coral sands, coal, etc (Komar, 1977). Further discussion on some available longshore sediment transport formulas is presented in Artagan (2006). In the development of the model, for the calculation of longshore sediment transport rates, the Kamphuis (1991) formula is utilized.

3.4 MODEL STRUCTURE

For the purpose of investigating long-term shoreline changes, a numerical model based on "one-line" theory has been developed in the Middle East Technical University, Civil Engineering Department, Coastal and Harbor Engineering Laboratory. Simply, the model requires several input data and gives an output of new shoreline orientation after a time step. The model structure is drawn in Figure 3.3.

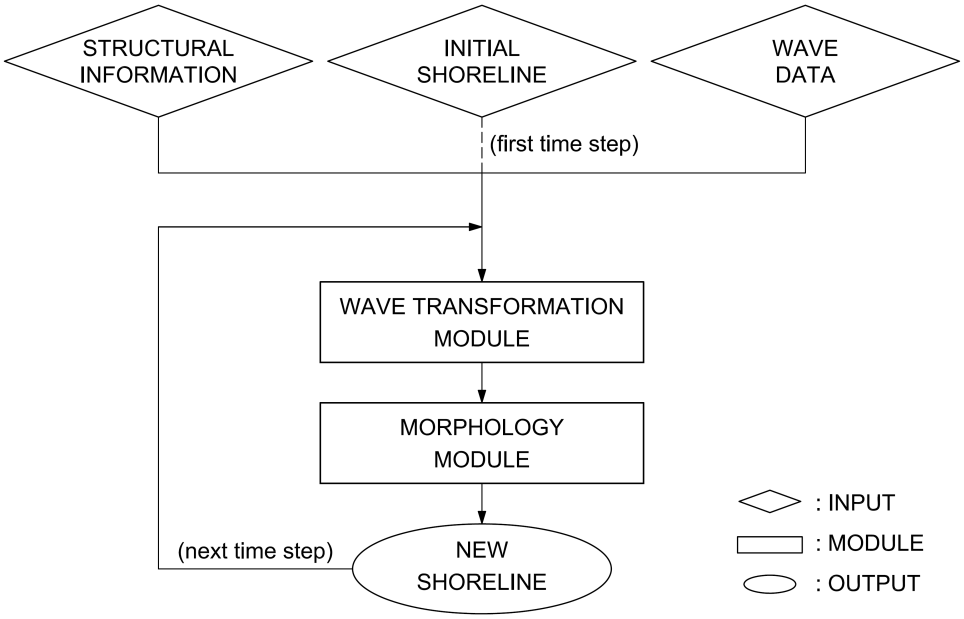

Figure 3.3 Model structure

The input data consists of site specific wave climate data, morphological features and existing or planned structural information (such as groins, breakwaters, beachfills). The wave data, a set of wave events including deep water wave heights, periods, angles, corresponding closure depths and frequencies of occurrence for each wave direction per year, is obtained from either a wave history data or a wind climate study depending on the available type of data recorded by local meteorological stations. Another major input is the initial shoreline orientation and

physical characteristics (such as median grain size in the surf zone, bottom slope or shape, berm height). The shoreline orientation is represented by an appropriate discretized shoreline. The last input data is the structural information such as the location and length of a groin or offshore distance of a detached breakwater. After all necessary input data is entered to the model, the shoreline is subjected to waves and its evolution in time is observed.

The spatial and temporal changes in shoreline orientation are computed by two modules; wave transformation and morphology modules. The wave transformation module is where wave refraction, shoaling, diffraction and breaking calculations are conducted to evaluate local breaking conditions for all grid cells along the discretized shoreline. In the module, the deep water wave parameters are first transformed into breaking wave parameters and then the effects of diffracting sources are considered and the breaking wave heights and angles within the sheltered zone of structures are re-calculated. The output data is used in the morphology module to calculate local sediment transport rates and changes in the shoreline due to alongshore sediment transport. The updated shoreline is used as input for the following time step and the same procedures continue until the end of simulation time.

3.5 NUMERICAL MODELLING

The governing equations (3.3) and (3.6) are solved numerically using a finite difference technique discretizing the shoreline into a finite grid and the simulation time into small time steps. Two schemes are available for finite difference; explicit and implicit. An explicit scheme is easier to programme compared with an implicit scheme due to the fact that boundary conditions and constraints become more complex to define in an implicit scheme (Şafak, 2006). However, an explicit scheme leads to more critical stability problems which effect the accuracy of the solution. In the development of GENESIS (Hanson, 1987) and ONELINE (Dabees and Kamphuis, 1998), an implicit scheme was adopted based on a given method by

Perlin and Dean (1978). In this study, an explicit scheme is utilized for programming shoreline evolution.

3.5.1 Grid System

The shoreline is discretized by a grid spacing of Δx and (N+1) calculation cells are formed, the position of shoreline is defined by (N+1) y coordinates of corresponding grids on the x axis (see Figure 3.4). For the calculation of y values at the next Δt time step, (N+2) Q values are needed. In a staggered grid system, the Q values are defined between two consecutive grid points whereas q values are defined at the grid points. The direction of sediment transport between two calculation cells is determined from the angle between wave crests and breaking bottom contour line such that if the waves are approaching to the coast from left to right looking from shore-side, it is assumed to have a positive transport and a negative one for the waves approaching from right to left (see Figure 3.4).

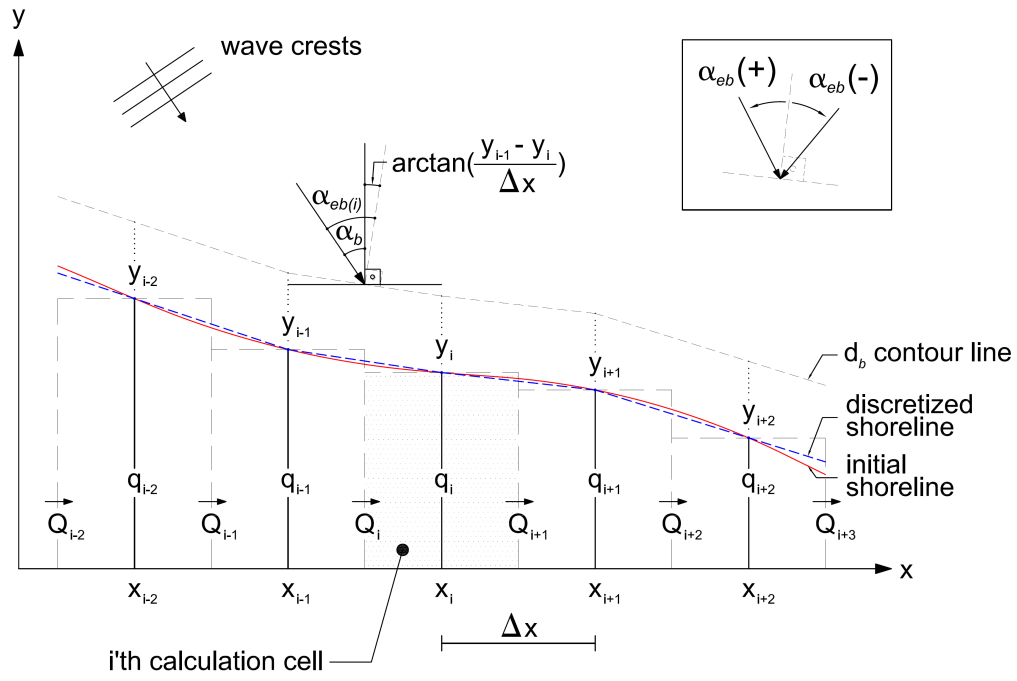

Figure 3.4 Grid system used for numerical modeling

The numerical solution of equation of mass conservation (3.3) using an explicit scheme is as follows;

$$y_i^* = y_i + \frac{\Delta t}{(D_c + B)} \cdot \left[\frac{Q_i - Q_{i+1}}{\Delta x} + q_i \right] \tag{3.8}$$

where the prime (*) indicates a quantity at the next time step and Δx is the distance between two consecutive grids. The shoreline position of a calculation cell Δt time later is calculated by the difference in longshore transport rates entering in (Q_i) and out (Q_{i+1}) of the cell and net cross-shore gain or loss (q_i) over the active profile, (D_{LT}+B). If there are no sources or sinks, q_i is taken to be equal to 0. Further confining the sediment transport only to longshore sediment transport (cross-shore or other sediment transport mechanisms are not considered), then the seaward limit of the active profile is taken as the depth where no longshore sediment transport exists. To be used in computations for shoreline evolution and bypassing around coastal structures (Şafak, 2006), this depth is defined as the limiting depth of longshore sediment transport (D_{LT}) and is related to wave breaking wave height (H_b), the key process in the longshore transport. It is given in equation (3.9) presented by Hallermeier (1978) where H_b and T are the breaking wave height and associated period respectively.

$$D_{LT} = 2.28 \cdot H_b - 68.5 \cdot \left(\frac{H_b^2}{gT^2}\right) \tag{3.9}$$

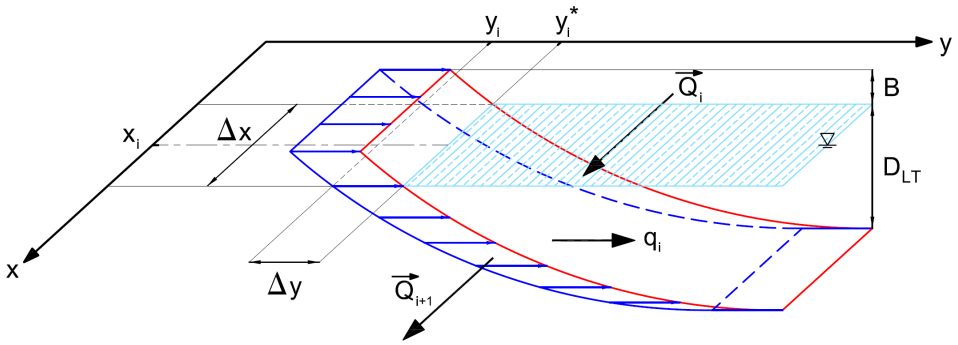

Figure 3.5 The i'th calculation cell in the numerical model

The i'th calculation cell in Figure 3.4 is drawn in detail in Figure 3.5 such that a section of shoreline with Δx length moves in cross-shore direction as backward or forward. Along the section, shoreline position is assumed to have a value of y, and y^* after Δt time.

To calculate sediment transport rates between two consecutive grids, the variables, introduced in the transport expression (3.6), changing alongshore have also (N+2) values. In most of the cases, all the parameters included in equation (3.6) except the breaking wave height, angle and bottom slope at breaking depth may be assumed identical to all grids. Under changing shoreline conditions, breaking wave angle (α_b) measured between the bottom contours and wave crests also changes. Then, the local breaking wave angle called as the effective breaking wave angle (α_{eb}) between two consecutive grid points is defined as;

$$\alpha_{eb(i)} = \alpha_b + \arctan\left(\frac{y_{i-1} - y_i}{\Delta x}\right) \tag{3.10}$$

where α_b is the breaking wave angle with respect to x axis (see Figure 3.4). The breaking wave height alongshore the discretized shoreline is obtained from a wave transformation procedure including shoaling, refraction, breaking and diffraction mechanisms.

3.5.2 Boundary Conditions

In order to link the modeled shoreline to the outside environment and to solve equation (3.3), the boundary conditions for either y or Q at the two lateral ends of the beach are essential. Commonly applied lateral boundary conditions are Neumann or radiation boundary condition that represents the natural beach condition where the change in shoreline position is negligibly small and Dirichlet boundary condition which represents for an impermeable shore-normal barrier where sediment transport rate is equal to zero. Another type of boundary condition

controls the cross-shore movement of shoreline as backward in case of seawall and as forward in case of tombolo formation behind detached breakwater.

The numerical solution of conservation of mass equation (3.8) requires (N+2) Q values for the calculation of (N+1) y values in time. Since the major parameter in the calculation of longshore sediment transport, the effective breaking wave angle is not defined at the two lateral ends, sediment transport rates at these ends are defined with respect to corresponding boundary condition. If the boundary holds for no significant shoreline change with time, $\frac{\partial y}{\partial t} = 0$, equation (3.3) then yields $\frac{\partial Q}{\partial x} = 0$ which may be expressed as $Q_1=Q_2$ or $Q_{N+2}=Q_{N+1}$. If a complete shore-normal barrier that interrupts the longshore sediment movement, exists at one end of the shoreline, then this condition can be expressed as $Q_1=0$ or $Q_{N+2}=0$.

The complete barrier lateral boundary condition can also be introduced as an internal constraint at any interior location in the grid system, to represent the applications of groins or jetties as coastal defense measures depending on their capacity of wave energy absorption and sediment transport blocking. The amount of sediment blocked by the structure is related to the seaward extent of the groin with respect to the critical offshore distance that corresponds to the depth of closure (Dabees, 2000). The amount of wave energy absorption capacity, which also controls the sediment blocking, is expressed with the permeability of the groin. The details of the calculations of bypassing and permeability conditions about groins in the developed model are discussed extensively by Şafak (2006).

3.5.3 Stability Criterion

The determination of the sizes of time interval (Δt) and grid spacing (Δx) depends on the stability parameter (R_s) when other parameters are kept constant in equation (3.12). For small breaking wave angles, the stability parameter is given as:

$$R_s \leq 0.5 \qquad (3.11)$$

where

$$R_s = \left[\frac{Q \cdot \Delta t}{\alpha_{eb} \cdot (\Delta x)^2 \cdot (D_c + B)} \right] \tag{3.12}$$

The stability parameter gives an estimate of the numerical accuracy of the solution such that accuracy increases with decreasing values of R_s (Hanson and Kraus, 1986).

3.6 WAVE TRANSFORMATION CALCULATIONS

The deep water significant wave parameters obtained from either a wave climate study or existing wave history data should be transformed into breaking conditions in order to be used in the longshore sediment transport expressions, (3.5) or (3.6). Wave transformation is governed by several processes like refraction, shoaling, diffraction, dissipation due to friction, dissipation by percolation, breaking, additional growth due to the wind, wave-current interaction and wave-wave interactions (CEM, 2003).

In the wave transformation calculations, small amplitude wave theory is used and two major mechanism; breaking (including bottom effects; shoaling and refraction) and diffraction are considered. First, breaking wave parameters, breaking height (H_b), angle (α_b), and depth (d_b) are calculated including the effects of refraction and shoaling. Then, the diffraction effects are considered and the breaking wave height (H_b) and angle (α_b) are modified to account for changes in wave patterns from each diffraction source at the breaking depth, d_b.

3.6.1 Wave Breaking

Waves approaching the coast increase in steepness as water depth decreases. When the wave steepness reaches to a limiting value, the wave breaks, dissipating energy and inducing nearshore currents and an increase in mean water level. Waves break

in a water depth approximately equal to the wave height. The surf zone is the region extending from the seaward boundary of wave breaking to the limit of wave uprush. Within the surf zone, wave breaking is the dominant hydrodynamic process (CEM, 2003). There are several methods for calculating breaking wave parameters. A comparison of these methods is available in Artagan (2006). The undiffracted wave height (H_b) is determined by solving equation (3.13) (CEM, 2003) iteratively for H_b,

$$H_b = (H_0)^{4/5} \cdot [C_{g0} \cdot \cos(\alpha_0)]^{2/5} \cdot \left[\frac{g}{\gamma_b} - \frac{H_b \cdot g^2 \cdot \sin^2(\alpha_0)}{\gamma_b^2 \cdot C_0^2} \right]^{-1/5} \qquad (3.13)$$

where H_b is the breaking wave height, H_o is the deep water significant wave height, α_0 is the deep water wave angle between wave crests and bottom contours, g is the gravitational acceleration (taken as 9.81 m/sec^2), γ_b is the breaker depth index given by (3.14) and assumed to be equal to 0.78, C_o and C_{go} are the deep water wave celerity and group celerity respectively and are calculated by equations (3.14), (3.16) and (3.17).

$$\gamma_b = H_b / d_b \qquad (3.14)$$

$$L_0 = 1.56 \cdot T^2 \qquad (3.15)$$

$$C_0 = L_0 / T \qquad (3.16)$$

$$C_{g0} = 0.5 \cdot C_0 \qquad \text{(for deep water waves)} \qquad (3.17)$$

L_o is the deep water wave length and T is the significant wave period. d_b is calculated from (3.14) replacing the values of γ_b and H_b. The breaking wave angle α_b is calculated from Snell's Law as a refraction equation (3.18).

$$\frac{\sin(\alpha_b)}{L_b} = \frac{\sin(\alpha_0)}{L_0} \tag{3.18}$$

The breaking wave length L_b is determined from equation (3.19) in which Gravity Wave Table (SPM, 1984) is introduced for the calculation of $tanh(kd_b)$ where the wave number k is equal to $2\pi/L$.

$$L_b = L_0 \cdot \tanh(k \cdot d_b) \tag{3.19}$$

In the model, for calculating the values of $tanh(kd_b)$, a subroutine including Gravity Wave Table is used.

3.6.2 Wave Diffraction

Wave diffraction is a process of wave propagation based on the lateral transfer of wave energy from points of greater to lesser wave height along the crest (perpendicular to the direction of wave propagation) of a wave that has a variable height along its crest (CEM, 2003). As in common with the other wave motions of sound, light, and electromagnetic waves, when the water waves encounter an obstacle during their propagation, they pivot about the edge of the obstacle and move into the shadow zone of the obstacle (Goda, 1985). The wave crest orientations and wave heights in the shadow zone are significantly changed. Therefore, the determination of diffracted wave heights and angles within the vicinity of coastal structures and formations like headlands is very important in order to accurate evaluation of shoreline evolution caused by longshore sediment transport.

The diffraction coefficient is defined by equation (3.20) as the ratio of the diffracted wave height at a point in the lee of the breakwater to the incident wave height at the tip of the breakwater.

$$K_d = H_d / H_i \tag{3.20}$$

In the shoreline change model, the incident wave height is assumed to be the undiffracted breaking wave height calculated at the breaker line. In order to determine diffraction coefficient and simulate interactions between shoreline and coastal structures in the model, either regular or irregular wave approach is utilized. Before utilizing an approach in the model, a comparison of the proposed methods has been made for a single groin. The background and comparison of the methods are given in next parts.

3.6.2.1 Regular Wave Diffraction

The simplest and classical approach for estimating wave diffraction is to consider regular or monochromatic waves in uniform depth interacting with a single straight breakwater (Briggs et al., 1995). The general problem of diffraction was originally solved by Sommerfeld (1896) for the diffraction of light passing the edge of a semi-infinite screen. Penny and Price (1952) showed that the same solution applies to the diffraction of linear surface waves on water of constant depth that propagate past the end of a semi-infinite thin, vertical-faced, rigid, impermeable barrier. Thus, the diffraction coefficients in the structure lee include the effects of the diffracted incident wave and the much smaller diffracted wave that reflects completely from the structure.

The diffraction coefficient for regular waves within the vicinity of a semi-infinite breakwater is expressed by;

$$K_d = f(\frac{r}{L}, \beta, \alpha_i) \tag{3.21}$$

where *r/L* is the ratio of radial distance from the breakwater tip to the point of interest to the wave length at the tip of breakwater, β is the angle between the breakwater alignment and this radial, and α_i is the incident wave angle between the extension of the breakwater alignment and incident wave direction (see Figure 3.6) (Penny and Price, 1952).

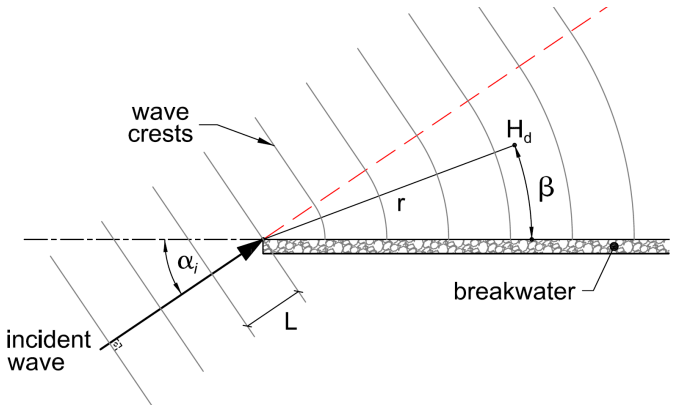

Figure 3.6 Wave diffraction, definition of terms (CEM, 2003)

Wiegel (1962) summarized the Penny and Price (1952) solution (3.21) and prepared conventional diffraction diagrams for approach angles varying by 15 degrees intervals from 15 to 180 degrees that can be found in Wiegel (1962) and the Shore Protection Manual (1984). Figure 3.7 shows Wiegel's (1962) results for an approach angle (α_i) of 60 degrees (SPM, 1984).

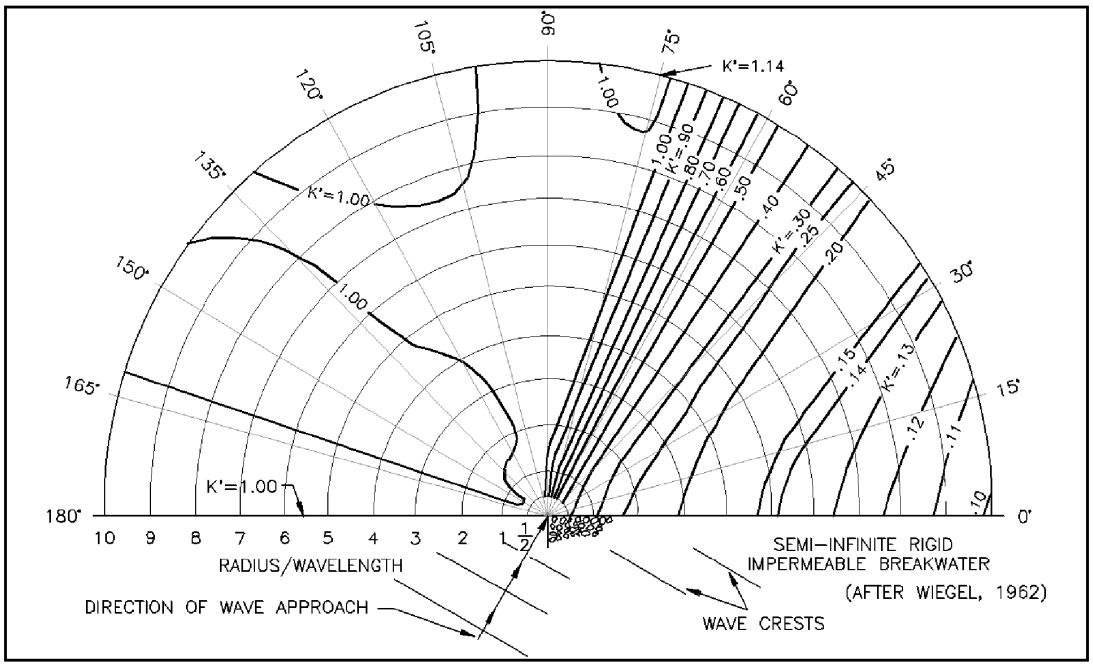

Figure 3.7 Diffraction diagram for regular waves, for an approach angle (α_i) of 60 degrees (SPM, 1984)

An interesting feature demonstrated by Figure 3.7 is that for this approach angle, the value of the diffraction coefficient along a line in the lee of the breakwater that extends from the breakwater tip in the direction of the approaching wave is approximately 0.5. This is true not only for the approach angle of 60 deg, but for any approach angle. Note also that for a given location in the lee of a breakwater, a one-dimensional spectrum of waves that comes from the same direction will undergo a greater decrease in height (energy density) for successively higher frequency waves in the spectrum. Increasing frequencies mean shorter wavelengths and consequently larger values of r/L (for given values of β and α_i). Thus the diffracted spectrum will have a shift in energy density towards the lower frequency portion of the spectrum (CEM, 2003).

To compute diffraction coefficient behind a groin with monochromatic theory in a numerical model, either the Fresnel integrals and several trigonometric functions must be evaluated (Kraus, 1984) or the diffraction coefficients should be determined from diagrams for corresponding grid points in the shadow zone of the groin which may require interpolations between diffraction contour lines and also for intermediate approach angles.

3.6.2.2 Irregular Wave Diffraction

Sea waves can not be adequately described by using the frequency spectrum alone. Irregular waves specified solely by the frequency spectrum would appear as so called long-crested waves which have straight, parallel crestlines. The patterns of random sea wave crests are composed of many component waves propagating in various directions. Therefore, the concept of directional spectrum is needed to be introduced to describe the state of superimposed directional components.

The previous discussion of wave diffraction was concerned with monochromatic waves. The effects of wave diffraction on an individual wave depend on the incident wave frequency and direction. Thus, each component of a directional wave spectrum will be affected differently by wave diffraction and have a different K_d

value at a particular point in the lee of a breakwater. The irregular wave diffraction methodology is simply based on the superposition of diffraction of several monochromatic waves having a range of representative frequencies and directions (CEM, 2003).

Goda, Takayama, and Suzuki (1978) developed diffraction calculation method and prepared diffraction diagrams for random sea waves introducing directional wave spectrum, which considers the structure as an obstacle blocking out a part of this spectrum. The effective diffraction coefficient is defined as follows;

$$(K_d)_{eff} = \left[\frac{1}{m_0} \cdot \int_0^{\infty} \int_{\alpha_{i,\min}}^{\alpha_{i,\max}} S(f,\alpha_i) \cdot K_d^2(f,\alpha_i) \cdot d\alpha_i \cdot df \right]^{1/2} \qquad (3.22)$$

where $(K_d)_{eff}$ denotes the diffraction coefficient of random sea waves (i.e., the ratio of diffracted to incident heights of significant or other representative waves), $K_d(f, \alpha_i)$ is the diffraction coefficient of component (regular) waves with frequency f and direction α_i, and m_0 is the integral (zero moment) of the directional spectrum, $\alpha_{i,max}$ and $\alpha_{i,min}$ are the limits of the spectral wave component directions, and $S(f, \alpha_i)$ is the spectral energy density for the individual components (Goda, 1985).

Goda (1985) states that the degree of directional spreading of wave energy, represented by spreading parameter (S_{max}) greatly affects the extent of wave refraction and diffraction. The deep water spreading parameter (S_{max0}) can be determined either from Figure 3.8 for a deep water wave steepness value (H_0/L_0) or from equation (3.23) where U is the wind speed and f_p denotes the frequency at the spectral peak which can be calculated from (3.24) for a given significant wave period (T).

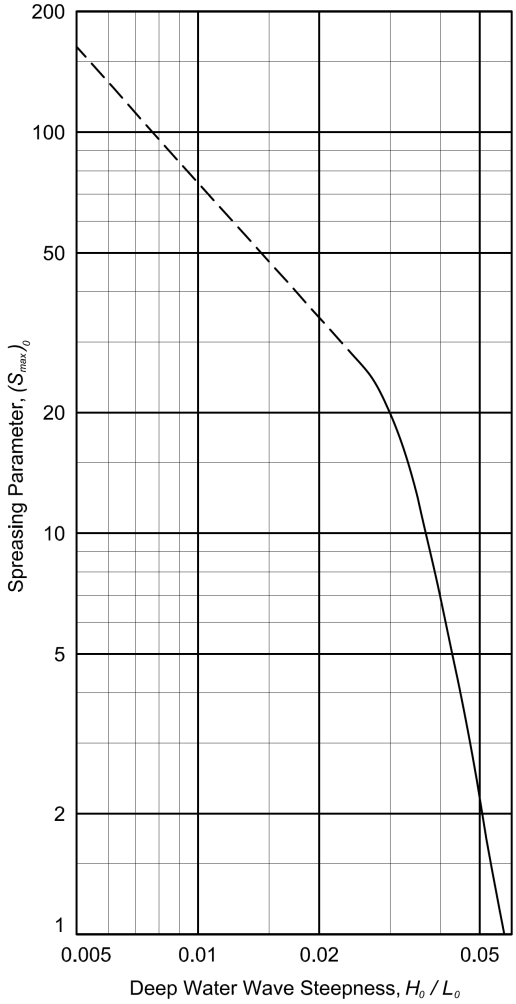

Figure 3.8 Relationship between spreading parameter and deep water wave steepness (Goda, 1985)

$$S_{\max 0} = 11.5 \cdot (2\pi \cdot f_p \cdot U / g)^{-5/2} \tag{3.23}$$

$$f_p = \frac{1}{1.05 \cdot T} \tag{3.24}$$

For engineering applications, until that time when the nature of the directional wave spectrum becomes clear on the basis of detailed field observations, Goda (1985) suggests the following values of spreading parameter (S_{max0}) in deep water given in Table 3.1.

Table 3.1 Directional spreading parameter in deep water (S_{max0}) for different wave types (Goda, 1985)

Wave Type	S_{max0}
Wind waves	10
Swell with short to medium decay distance (with relatively large wave steepness)	25
Swell with medium to long decay distance (with relatively large wave steepness)	75

The spectral diffraction diagrams are given for different S_{max} (spreading parameter at the tip of the diffracting source) values (10 and 75) and in the near and distant areas of a semi-infinite breakwater. When using these diagrams, the effect of wave refraction upon the parameter S_{max0} must be taken into account, because most breakwaters are built in relatively shallow water compared to the predominant wave length, and the directional wave spectrum has transformed from that to corresponding to deep water. The effect of wave refraction upon the parameter S_{max0} can be estimated from the curves in Figure 3.9 for given deep water spreading parameter (S_{max0}), wave length (L_o) and deep water wave angle (α_0) (Goda, 1985).

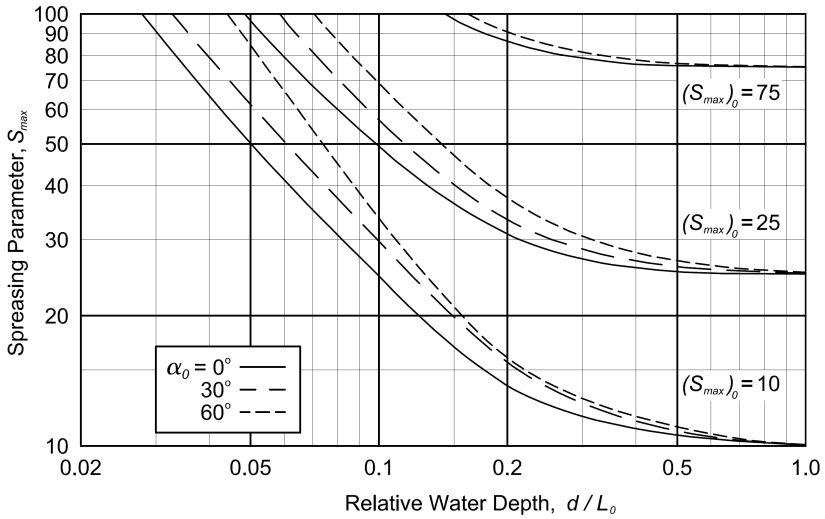

Figure 3.9 Estimation of spreading parameter (S_{max}) in shallow water area (Goda, 1985)

In Figure 3.10, the diffraction diagram for irregular waves in the near area of a semi-infinite breakwater is given. The diffraction coefficients for spreading parameters other than S_{max} =10 and S_{max} =75 are interpolated. The angle of approach direction in these diagrams is normal to the breakwater orientation. In case of oblique incidence of waves, the diffraction coefficient can be calculated by rotating the axis of the breakwater while keeping the wave direction and the coordinate axes at their original positions. This technique produces some error when the angle between the principal direction of wave approach and the line normal to the breakwater exceeds ±45 degrees (Goda, 1985). However, this error may be neglected during one-dimensional modeling of shoreline changes, because the "one-line" theory works well with small breaking wave angles. The diagrams show also a small change in the peak period ratio as the waves extend into the breakwater lee (see Figure 3.10). For monochromatic waves the wave period would not change.

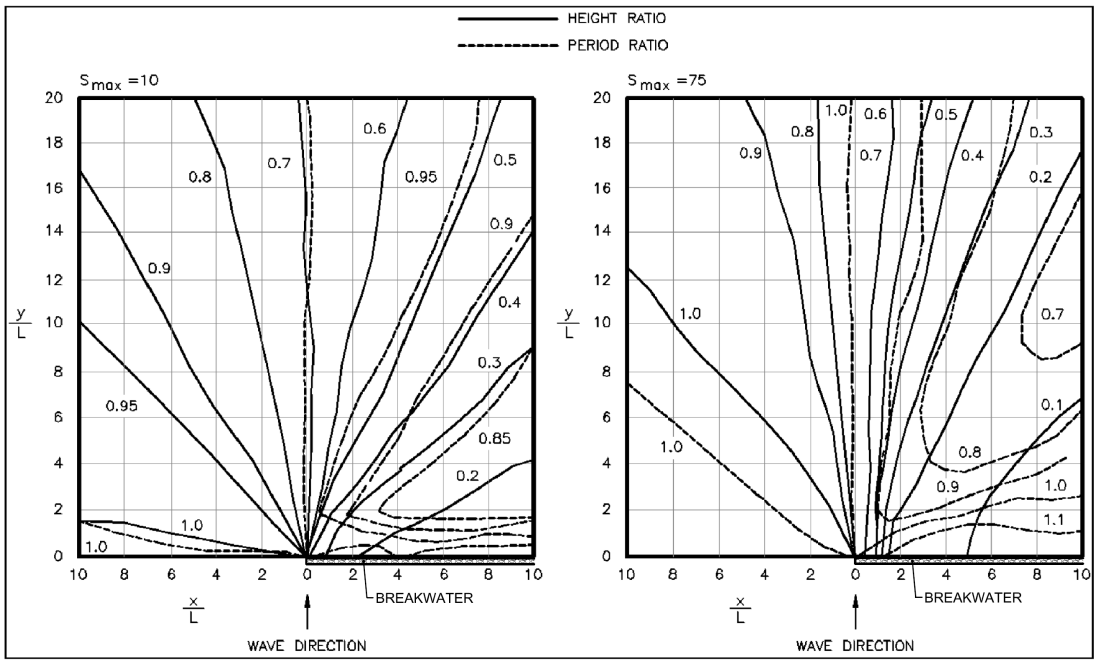

Figure 3.10 Diffraction diagram for random sea waves of normal incidence in the near area of a semi-infinite breakwater (Goda, 1985)

As shown in Figure 3.10, the effective diffraction coefficient values are quite different from those of regular waves. For example, the diffraction coefficient of random waves along the boundary of the geometric shadow (or the straight line from the tip of the breakwater parallel to the wave direction) takes the value of about 0.7, while regular wave diffraction theory gives a diffraction coefficient of about 0.5. The difference between the predictions increases in the sheltered area behind the breakwater, and would result in an underestimation of wave height there if diagrams for regular wave diffraction were employed. Therefore, direct application of conventional diagrams prepared for regular waves with constant period and single directional component to real situations is not recommended and may lead erroneous results (Goda, 1985).

The determination of diffraction coefficients using irregular wave approach is not effective with the direct use of diagrams in numerical modeling. For numerical modeling in the computer medium, approximate equations are obtained by means of regression analyses of these diagrams and relative figures. Some of these sets of equations are available in Kraus (1984), Leont'yev (1999) and Kamphuis (2000).

3.6.2.2.1 Kraus's (1984) Method

The method is based on considerations of the relative incident wave energy penetrating into the shadow zone. The cumulative relative wave energy, $P_E(\theta)$, at a point in the shadow zone of a diffracting source depends on the angle θ measured counterclockwise from the principal wave direction to the point and the spreading parameter (S_{max}) at the tip of the source. The cumulative distribution curves for S_{max}=5, 10, 25, and 75 are given in Figure 3.11.

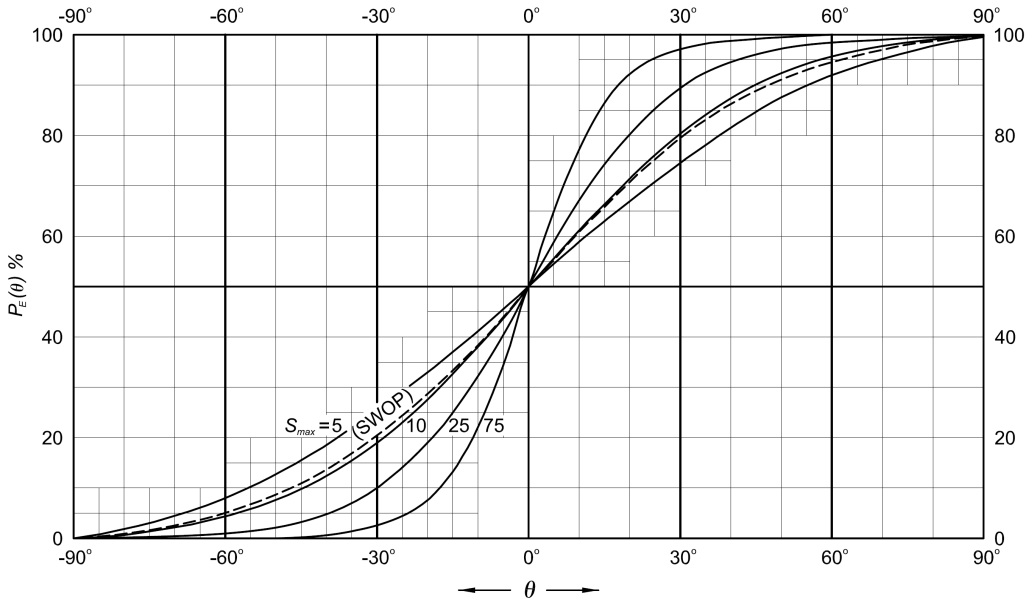

Figure 3.11 Cumulative distribution of relative wave energy with respect to azimuth from wave direction (Goda, 1985)

For the purpose of the computer routine, following approximate best-fit interpolative equations (3.25)-(3.27) are given to describe the curves in Figure 3.11 (Kraus, 1984). In equations (3.25)-(3.27), Kraus (1984) introduces dimensionless parameters, W and A, to find the cumulative relative wave energy, $P_E(\theta)$. In Figure 3.12, the shadow angle (θ) varies from $-\pi/2$ to $\pi/2$ and is defined as negative inside the shadow zone and positive outside.

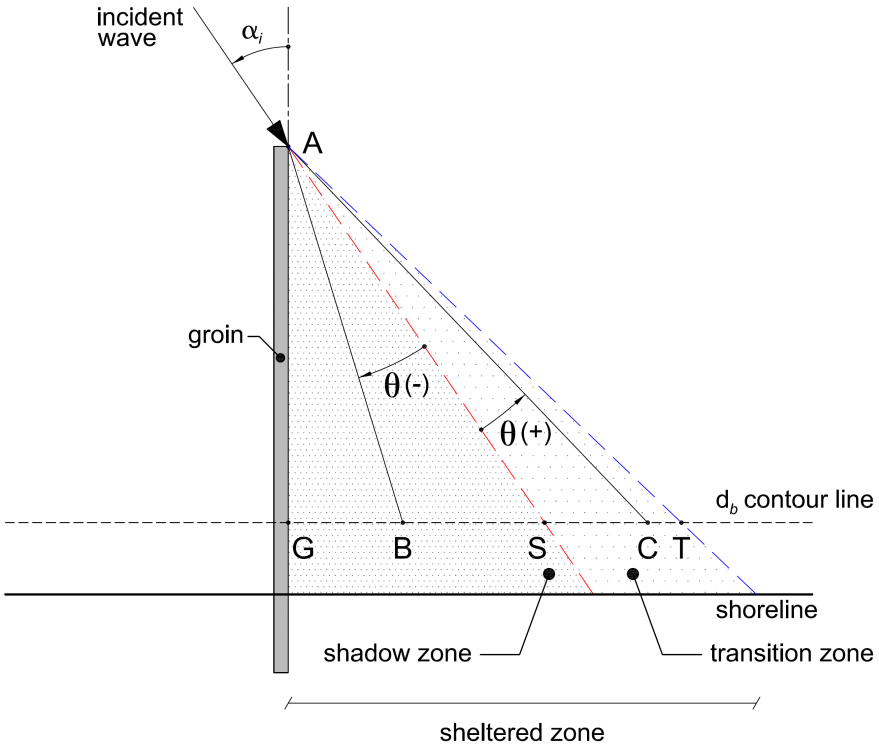

Figure 3.12 Definition sketch of wave diffraction near a groin

$$W = 5.31 + 0.270 \cdot S_{\max} - 0.000103 \cdot S_{\max}^2 \tag{3.25}$$

$$A = \frac{S_{\max}}{W} \cdot \theta \quad (\theta \text{ in radians}) \tag{3.26}$$

$$P_E(\theta) = 50 \cdot [\tanh(A) + 1] \qquad (\%) \tag{3.27}$$

Kraus states that equations (3.25)-(3.27) for the calculation of cumulative relative wave energy agree with the Figure 3.11 with a maximum error of about 2% of full scale in the interval $10 \leq S_{max} \leq 75$.

With S_{max} given at the tip, the diffraction coefficient $K_d(\theta)$ for a given point in the lee of a diffracting source is then calculated from equation (3.28).

$$K_d(\theta) = \sqrt{\frac{P_E(\theta)}{100}} \tag{3.28}$$

The aforementioned procedure is also used by GENESIS (Hanson and Kraus, 1989) and LITLINE (Danish Hydraulics Institute, Denmark) for the calculation of diffraction coefficients. However, the effect of wave incidence angle is neglected and refracted S_{max} values are obtained from the curves given by 30 degrees of approach angle in Figure 3.9 (Hanson, 1987; LITLINE).

3.6.2.2.2 Leont'yev's (1999) Method

Based on the theory of Goda et al. (1978) for irregular waves, Leont'yev (1999) introduces a set of equations for the calculation of diffraction coefficient K_d in the shadow zone behind the structures. As described in above procedure (Kraus, 1984) the diffraction coefficient depends on the spreading parameter (S_{max}) and the shadow angle θ. Leont'yev (1999) states that in most practical cases a typical value of S_{max} falls in the range 25 - 75 m and variations of S_{max} within these limits have a rather weak influence on the K_d value, therefore to simplify the calculations, the uniform value $S_{max} = 50$ is used and approximate changes in K_d in the sheltered zone of diffracting sources with θ (in radians) are given by the following set of equations:

$$K_d = \begin{cases} 1 & \theta \le -\pi/6 \\ 0.1 \cdot (\theta + \pi/6) + \cos^3(\theta + \pi/6), & -\pi/6 \le \theta \le \pi/2 \\ 0.087 \cdot (3 - 4\theta/\pi), & \pi/2 \le \theta \le 3\pi/4 \\ 0 & 3\pi/4 \le \theta \end{cases} \tag{3.29}$$

On the contrary to the definition of the shadow angle θ in Kraus (1984), Leont'yev defines θ as positive in the shadow zone and negative in the illuminated region. The boundary of the wave shadow area where the value of K_d approaches to 1 corresponds to a shadow angle $\theta = -\pi/6$. On the line coinciding with the wave direction, where $\theta = 0$, K_d is close to 0.7 (Leont'yev, 1999).

3.6.2.2.3 Kamphuis's (2000) Method

Goda (1985) assumes that all the energy in the directional spectrum of incoming wave ray at a structure for which $\alpha<\alpha_i$ is blocked by the structure and removed from the spectrum. Along the shadow line, half of the incident wave energy is assumed to be lost, and since the wave energy is directly proportional to the second power of wave height, along the shadow line H is found as; $H = \sqrt{2}H_i = 0.71H_i$, where H_i is the incident wave height (Kamphuis, 2000). Using Goda's method and some additional assumptions, Kamphuis introduces simple expressions for diffraction behind a groin relating the wave energy reaching a point behind the groin to the angle θ.

$$K_d = 0.71 + 0.0093 \cdot \theta + 0.000025 \cdot \theta^2 \quad \text{for} \quad -90 \le \theta \le 0 \tag{3.30}$$

$$K_d = 0.71 + 0.37 \cdot \sin(\theta) \quad \text{for} \quad 0 \ge \theta \ge 40 \tag{3.31}$$

$$K_d = 0.83 + 0.17 \cdot \sin(\theta) \quad \text{for} \quad 40 \ge \theta \ge 90 \tag{3.32}$$

As θ approaches to 90 degrees, K_d converges to 1.0, but in theory measuring such an angle from the shadow line of the groin is not possible on a straight beach for a single groin. This case leads some problems that will be discussed later.

3.6.2.2.4 Proposed Diffraction Method

In the numerical model, a modified diffraction methodology based on Kamphuis's (2000) method has been followed. The diffraction coefficient is computed for the shadow angle (θ) at the point of interest in the shadow zone of the structure from equation (3.30). To compute the diffraction coefficient K_d in the transition zone, the trend of K_d coefficient in the shadow zone is linearly extended up to a value 1.0 accepting the fact that diffraction coefficient should be equal to 1.0 beyond the sheltered zone. Using the diffraction coefficients $K_{d,G}$ and $K_{d,S}$ computed at points G (at the groin) and S (at the end of shadow zone) respectively (see Figure 3.12), the

diffraction coefficient $K_{d,C}$ at any point C in the transition zone of the structure is computed from equation (3.33);

$$K_{d,C} = K_{d,S} + [SC] \cdot \left(\frac{K_{d,S} - K_{d,G}}{[GS]} \right) \quad \text{for} \quad \theta > 0 \tag{3.33}$$

where [*SC*] is the distance between the point of interest to the end of shadow zone on the breaker line and [*GS*] is the alongshore length of shadow zone on the breaker line. The end of the transition zone is determined by where the diffraction coefficient computed from equation (3.33) reaches to value of 1.0. Therefore, the length of sheltered zone on the breaker line where the diffraction coefficient changes is governed by the incident wave angle at the seaward tip of the structure (α_i) and the trend in the variation of *Kd* in the shadow zone. The final diffracted breaking wave height in the sheltered zone is computed by the following equation.

$$H_{bd} = K_d \cdot H_b \tag{3.34}$$

The determination of another breaking parameter controlling the longshore sediment transport, wave breaking angle in the vicinity of diffracting structures is explained by the combined refraction-diffraction phenomena, which is discussed in the forthcoming parts.

3.6.2.3 Comparison of Methods

The diffraction is the key process that governs the shoreline changes in the shadow zones of coastal structures. It has significant effects on the wave heights and angles, which are the main parameters of longshore sediment transport expression. To decide on the methodology that will represent the diffraction mechanism in the numerical model, a comparison has been made for the alongshore variation of diffraction coefficient at the downdrift side of a groin (see Figure 3.13) calculated with available methodologies; Goda et al. (1978), SPM (1984), Kraus (1984), Leont'yev (1999) and Kamphuis (2000) together with the proposed method.

The comparison of methods is made for a single groin having 200 meters apparent length on a straight shoreline with a bottom profile known as Dean's Profile (1977). Since it is said in Wang et al. (2002) that Kamphuis's formula (1991) for longshore sediment transport gives more consistent predictions for low-energy events (less than 1 m in wave height), the deep water wave height, period and approach angle (measured between wave crests and straight bottom contour lines) are given as 1.0 meter, 4.0 seconds and 17.3 degrees of which value drops to 15.0 degrees at the tip of the groin due to bottom effect respectively. The simulation durations are 100 hours and 1000 hours to represent short- and long-term changes. The deep water wave steepness has a value of 0.040 which is acceptable for Turkish coasts (Ergin and Özhan, 1986). The respective spreading parameter at the tip of the groin is found to have a value of 11.2 from Figure 3.9. The shadow zone extends 46 meters from groin to right on the breaking line defined by 5 grids with 10 meters grid spacing. The median grain size diameter and the berm height are assumed as 0.4 millimeters and 2.0 meters respectively.

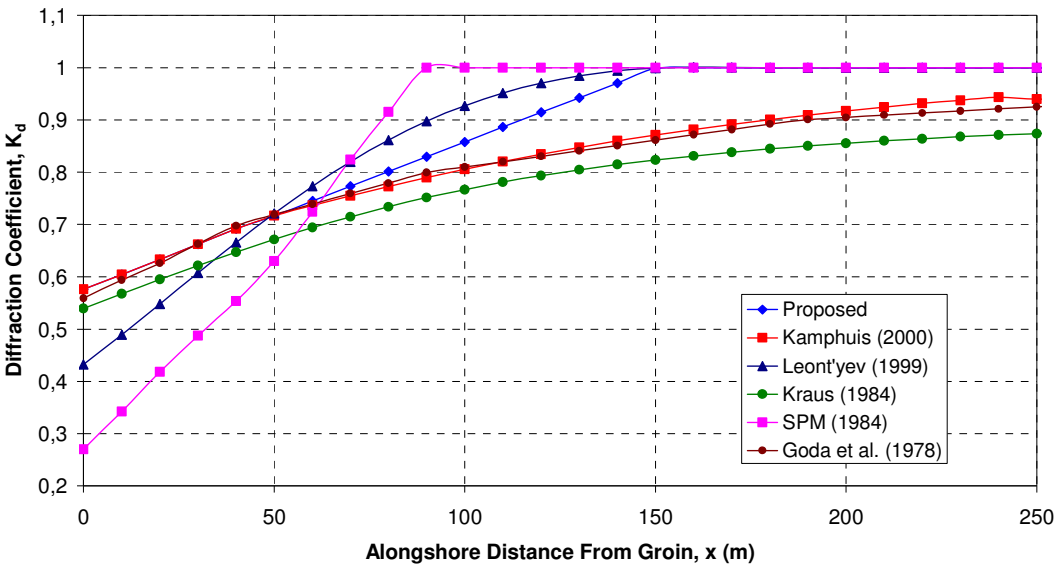

Figure 3.13 The alongshore variation of diffraction coefficient at the downdrift side of the groin

As shown in Figure 3.13, the regular wave diffraction theory (SPM, 1984) underestimates the diffraction coefficients in the shadow zone and overestimates in the transition zone when compared with irregular wave diffraction theory. The results of methodologies representing irregular wave diffraction theory differ from each other such that K_d computed from Leont'yev's expression (1999) reaches to the value of 1.0, which means the alongshore end of sheltered zone, at a distance from groin, whereas the expressions given by Kraus (1984) and Kamphuis (2000) computes K_d smaller then 1.0 till the end of modeled shoreline and theoretically converge to 1.0 for $\theta = 90^o$. This situation leads to a problem of that the sediment mass is not conserved within the control volume of the model and the effects of diffraction process is felt at all downdrift grid points alongshore no matter how far they are from the source of diffraction. In order to get rid of this conservation and extended diffraction effect problem, Leont'yev's expression may be utilized, yet, this expression is derived for a uniform value of spreading parameter $S_{max} = 50$ and thus may underestimate K_d in the shadow zone for random waves with small spreading parameters like $S_{max} = 10$. In the sheltered zone of the groin, Kamphuis's expression is in good agreement with irregular wave diffraction diagrams.

Furthermore, to observe the effects of different diffraction methods on the shoreline change at the downdrift of the same groin, short- and long-term shoreline changes are given in Figures 3.14 and 3.15 respectively. The methodologies considered are; SPM (1984), Kraus (1984), Leont'yev (1999) and Kamphuis (2000) together with the proposed method. Since the alongshore variation of the diffraction coefficient (K_d) obtained from the irregular wave diffraction diagrams (Goda et al., 1978) is almost same with the one obtained from Kamphuis's (2000) method (see Figure 3.13), these diagrams (Goda et al., 1978) are not considered.

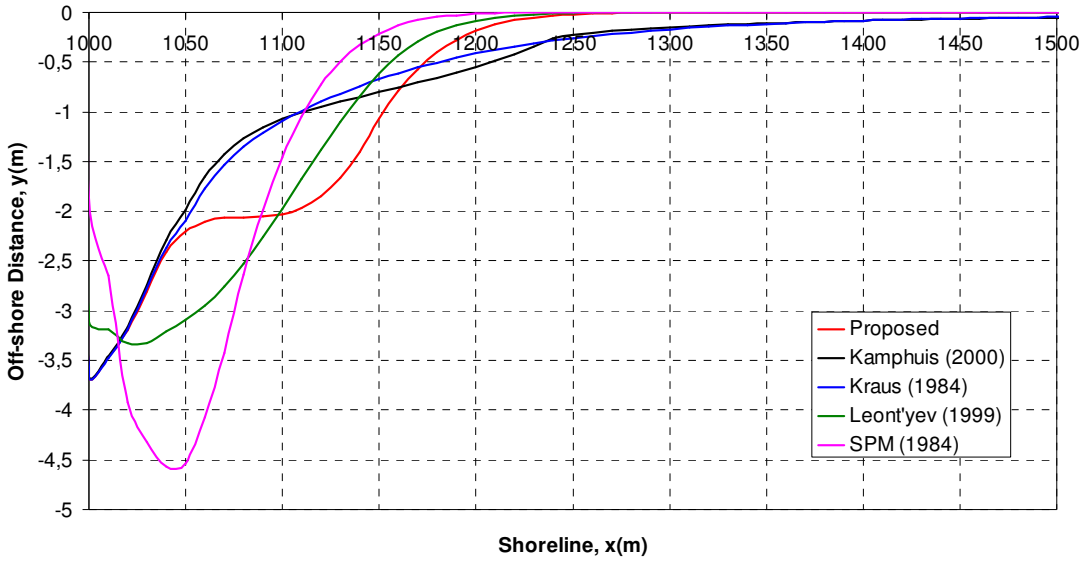

Figure 3.14 The shoreline change at the downdrift side of the groin after 100 hours

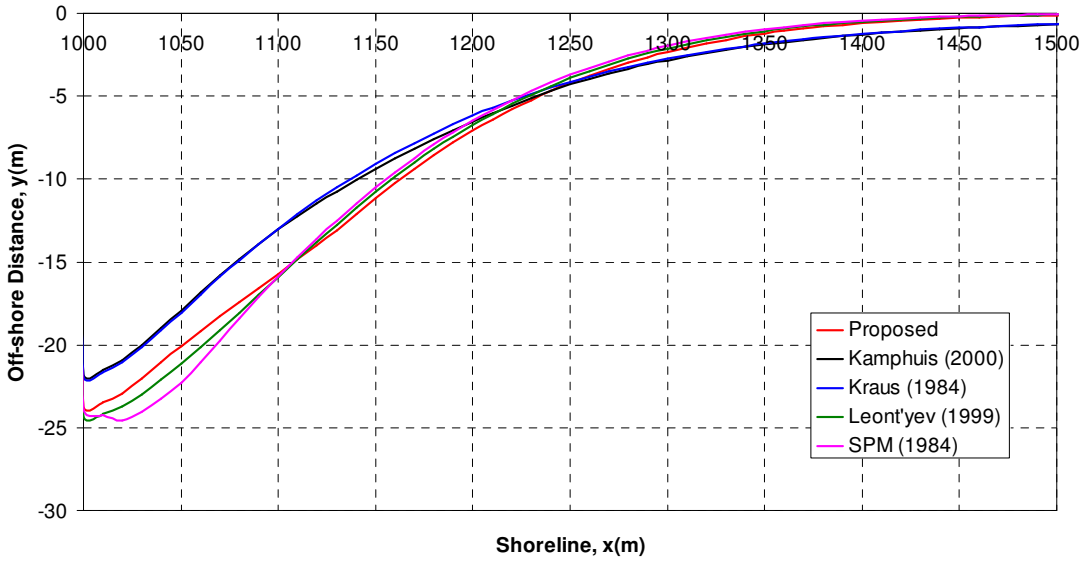

Figure 3.15 The shoreline change at the downdrift side of the groin after 1000 hours

As shown in Figure 3.14, in short term, the methodology applied governs the shoreline change in the sheltered zone of the groin. However, after 1000 hours which is not long enough considering "one-line" theory's limitations, the shoreline tends to have an equilibrium planform regardless of the diffraction methodology

utilized in the model (see Figure 3.15). The results of shoreline changes obtained from different diffraction methods show similarity both quantitatively and qualitatively.

Concluding from above discussions, in order to represent wave diffraction phenomena within the sheltered zones of shore-normal diffracting coastal structures (groins, jetties etc.) in the numerical model, the proposed method is utilized. In comparison with the other methods presented (especially the direct use of diagrams), the method applied is simpler, eliminates the conservation of mass and extended diffraction effect problems and gives results match well with the results of other methods in terms of long-term shoreline changes.

3.6.3 Combined Refraction and Diffraction

In cases where the depth is relatively constant between the tip of the structure and the point under consideration that is the breaker line in the model, the diffraction analyses discussed above are adequate to define the resulting wave conditions. However, if the depth changes significantly, then wave amplitudes will change because of shoaling effects. If the harbor bottom contours are not essentially parallel to the diffracting wave crests, then wave amplitudes and crest orientations will be affected by refraction (CEM, 2003).

Where depth changes in the lee of a diffracting source are sufficient for combined refraction and diffraction effects to be significant, the resulting wave height and direction changes can be investigated by either a numerical or a physical model study (CEM, 2003). Examples of such numerical model studies and some sophisticated methods for the calculation of combined refraction-diffraction in the lee of a structure are available in Berkhoff (1972), Liu and Lozano (1979), Radder (1979), and Liu (1982). Physical models that investigate the combined effects of refraction and diffraction are also routinely conducted (see Hudson et al. 1979).

Dabees (2000) states that the linear diffraction theory developed for water of constant depth (pure diffraction) predicts circular patterns of diffracted wave fronts, yet, shoaling and refraction due to varying water depths play an important role in modifying wave patterns behind structures (see Figure 3.16). Field studies shows that wave amplitude dispersion in shallow water changes the circular wave pattern into an arc of decreasing radius (Weishar and Byrne, 1978).

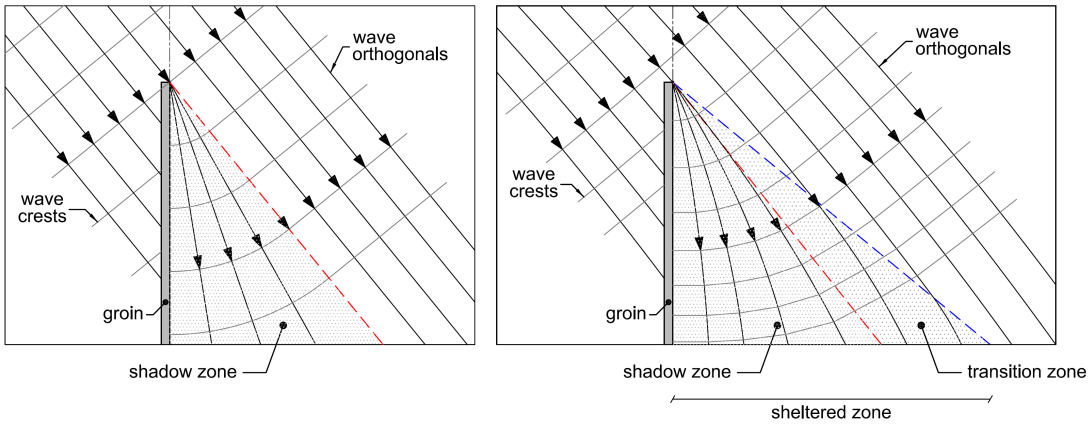

Figure 3.16 Illustration of pure diffraction and combined refraction-diffraction processes (modified from Dabees, 2000)

To consider combined refraction-diffraction effect in the lee of a diffracting source, the breaking wave angle, which is an important parameter in determination of the longshore sediment transport and is calculated from Snell's Law (3.18), is reduced due to diffraction in the shadow and transition zones. The end of the transition zone is defined previously as the point where K_d is equal to 1.0 again.

The methodology considering the two physical phenomena, refraction and diffraction, treated in GENESIS by Hanson (1987) is summarized in three steps;

- Waves are calculated from deep water to breaking depth, including the effects of refraction and shoaling. The influence of structure is ignored.

- The calculated breaking wave heights at the location affected by diffraction are recalculated using the wave height at the location of the tip of diffracting structure and an appropriate diffraction coefficient.

- Wave refraction from the diffracting tip to a specified location inside the shadow region, is determined with Snell's Law (3.18).

Another approach to consider the effect of diffraction on breaking wave angles in the sheltered zones of the structures is introduced by Kamphuis (2000) such that the diffracted breaking wave angle is simply related to the undiffracted breaking angle and the diffraction coefficient. In Figure 3.17, the diffracted breaking wave angles in the sheltered zone of a groin are illustrated.

The diffracted breaking angle behind a groin for any point inside and outside the shadow zone is found from following equation;

$$\alpha_{bd} = \alpha_b \cdot K_d^{0.375} \tag{3.35}$$

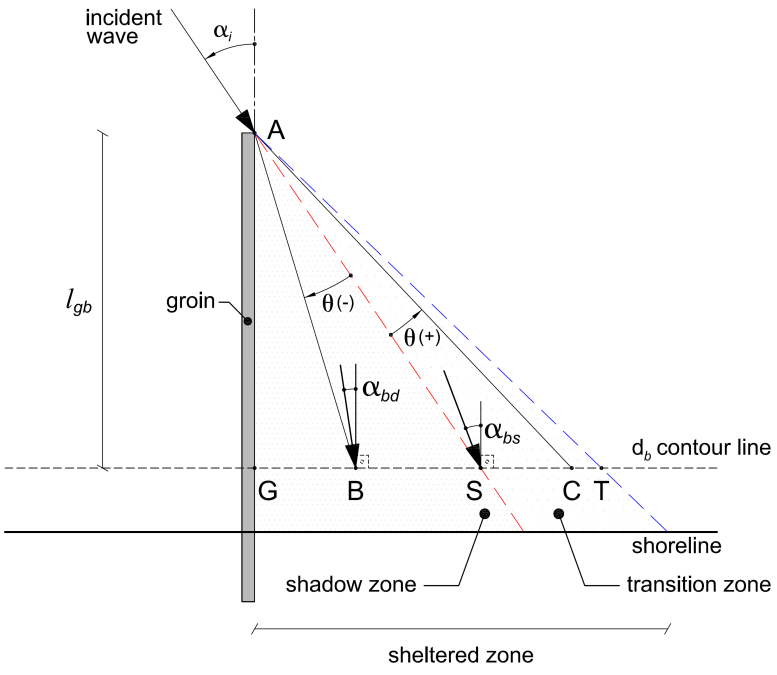

Figure 3.17 Diffracted breaking wave angles in the sheltered zone of a groin

Kamphuis (2000) states that inside the shadow zone, a further decrease in the breaking angle, resulting directly from wave diffraction, must be taken into account. The wave from the end of the groin according to the equation (3.35) will have a breaking angle of

$$\alpha_{bs} = \alpha_b \cdot (0.71)^{0.375} = 0.88 \cdot \alpha_b \tag{3.36}$$

Since the breaking angle at the structure is zero, a simple proportionality ratio is introduced so that for

$$\theta < 0 \quad \text{and} \quad \frac{[GB]}{l_{gb}} < \frac{1}{2}\{\tan(\alpha_i) + \tan(0.88 \cdot \alpha_b)\} \tag{3.37}$$

the adjusted breaking angle is

$$\alpha_{bd} = \alpha_b \cdot K_d^{0.375} \cdot \left[\frac{2 \cdot [GB]}{l_{gb} \cdot \{\tan(\alpha_i) + \tan(0.88 \cdot \alpha_b)\}} \right] \tag{3.38}$$

where l_{gb} is the groin length from the seaward tip of groin to the breaking location, α_i is the incident wave angle at the seaward tip of the groin, α_b is the undiffracted breaking angle, [*GB*] is the distance away from the groin and α_{bd} is the diffracted wave angle (see Figure 3.17).

The variation of breaking wave angle at the downdrift side of a 200 meters long groin is given for an incidence wave angle of 30 degrees and the effects of refraction and diffraction both separately and in combination which is the actual case behind a groin is illustrated in Figure 3.18.

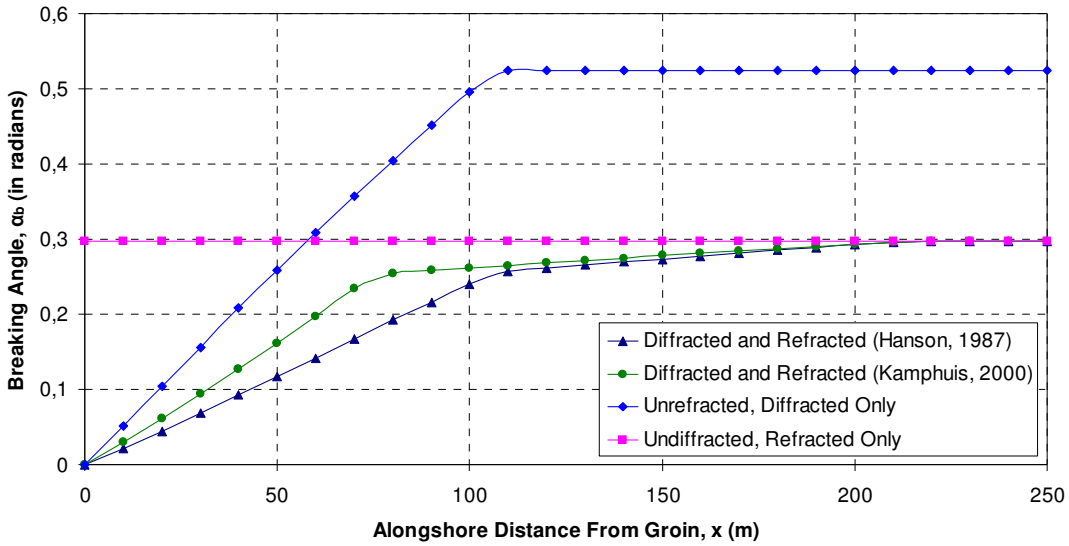

Figure 3.18 The alongshore variation of breaking wave angle at the downdrift side of the groin

As shown in Figure 3.18, the variations of the breaking wave angle in the sheltered zone of a groin for two idealized cases where it is assumed that only refraction or only diffraction process exists, are given to stress that the breaking wave angle found from Snell's Law (3.18) decreases further in the sheltered zone of the groin due to diffraction effect when considering combined refraction-diffraction process. The alongshore distance to the end of shadow zone (where $K_d = 0.71$) and to the end of the transition zone at the breaker depth from the groin is about 100 and 200 meters respectively. In the shadow zone, Kamphuis's (2000) combined refraction-diffraction methodology computes smaller values for the breaking wave angle than the methodology given in Hanson (1987), whereas in the transition zone they compute almost the same values for the breaking wave angle. In the numerical model, Kamphuis's (2000) methodology providing a simpler approach to compute the diffracted breaking wave angles is utilized.

3.7 GROINS AS SHORE PROTECTION MEASURES

Groins are the oldest and most common shore-connected, beach stabilization structures which are usually perpendicular or nearly at right angles to the shoreline and relatively short when compared to navigation jetties at tidal inlets. Groins are constructed to maintain a minimum, beach width for storm damage reduction or to control the amount of sand moving alongshore. Modern coastal engineering practice is to combine beach nourishment with groin construction to permit sand to begin immediately to bypass the groin field. Due to many examples of poorly designed and improperly sited groins caused by lack of understanding of their functional design, or failure to implement the correct construction sequence, or failure to fill up the groin compartments with sand during construction, or improper cross-sectional shape, the use of groins for shore protection is discouraged by coastal zone management policies in many countries (CEM, 2003).

The purpose of a groin field (series of groins) is to divide a shoreline into short sections that can reoriginate themselves with respect to the incoming waves (Kamphuis, 2000). For the proper functioning of shore-normal groins, SPM (1984) recommends a spacing ratio (X_g/Y_g) between 2.0 to 3.0 where X_g is the spacing between the groins and Y_g is the groin length measured from inital shoreline (see Figure 3.19). Groins that are spaced too closely cause sediment to bypass the compartments between groins. Spacing groins too far apart allows erosion of beach material between the groins. Therefore, an optimum design should consider both facts that a groin field should have the maximum sediment entrapment capacity while the amounts of erosion in groin compartments and at the downdrift of the groin field are in allowable limits.

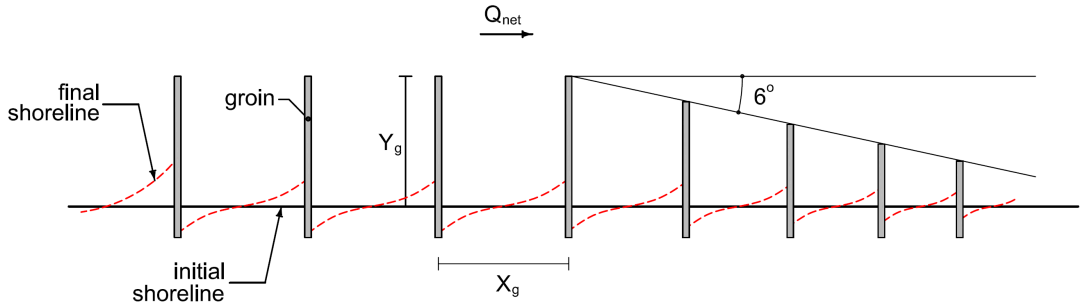

Figure 3.19 Definition sketch for a groin field

Another recommendation about functional design of groin fields, which is also illustrated in Figure 3.19, is that groin lengths are decreased along a line converging to the shoreline from the last full-length groin in the direction of net longshore sediment transport (Q_{net}), making an angle of about 6 deg with the natural shoreline and reducing the spacing to maintain the same X_g/Y_g ratio (2.0-3.0) used in the design (CEM, 2003). The principle of groin shortening is employed at the end of groin systems in order to develop a transition between the groin system and the adjacent natural beach and to reduce downdrift erosion. Bruun (1952) indicates that in a long series of groins, the shortening should probably be carried out on the updrift side also, to insure a smooth passage to the unprotected coast. He further indicates that if the series consists only of a few groins, the shortening should start with the second groin from the updrift end. This would result in all the groin system being a transitional section. Kressner (1928) found in model tests that only three or four groins need to be shortened at the downdrift end of the system.

To observe the effects of spacing ratios on the performance of a groin field, sample simulations are carried out with the numerical model developed for different sets of wave data input given Table 3.2 and for different spacing ratios as X_g/Y_g = 1.0, 2.0, 3.0, 4.0, 5.0 and 6.0. For each wave data set, the deep water wave approach angle (degrees measured between wave crests and straight bottom contour lines), wave frequency and steepness are kept constant and taken as 45 degrees, 5000 hours and 0.042 respectively, whereas the deep water wave height and period are as given in Table 3.2. The groin field is composed of 5 impermeable shore-normal groins 50

meters long each with a spacing varying from 50 meters to 300 meters. The sediment entrapment capacity of the groin field for each spacing ratio and at each wave set is determined with the net area of sediment entrapped (A_n) found simply from the algebraic sum of areas of accretion (+) and erosion (-) in groin compartments (see Figure 3.20).

Table 3.2 Wave data sets used in sample simulations

	H_0 (m)	T (sec)	α_0 (deg)	f (hrs)
Wave Set-1	0.8	3.5	45	5000
Wave Set-2	1.0	4.0	45	5000
Wave Set-3	1.2	4.3	45	5000
Wave Set-4	1.5	4.8	45	5000

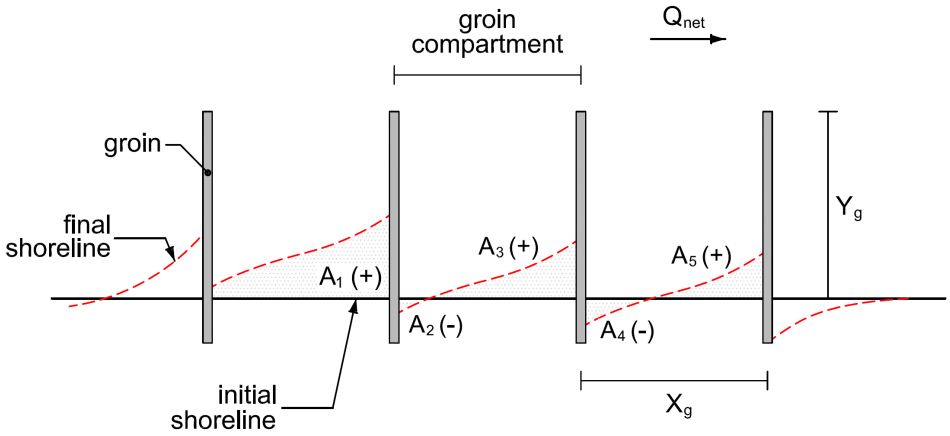

Figure 3.20 Areas of accretion and erosion in groin compartments

For each wave set, the changes in the net area of sediment entrapped as the spacing between groins is increased are illustrated in Figure 3.21.

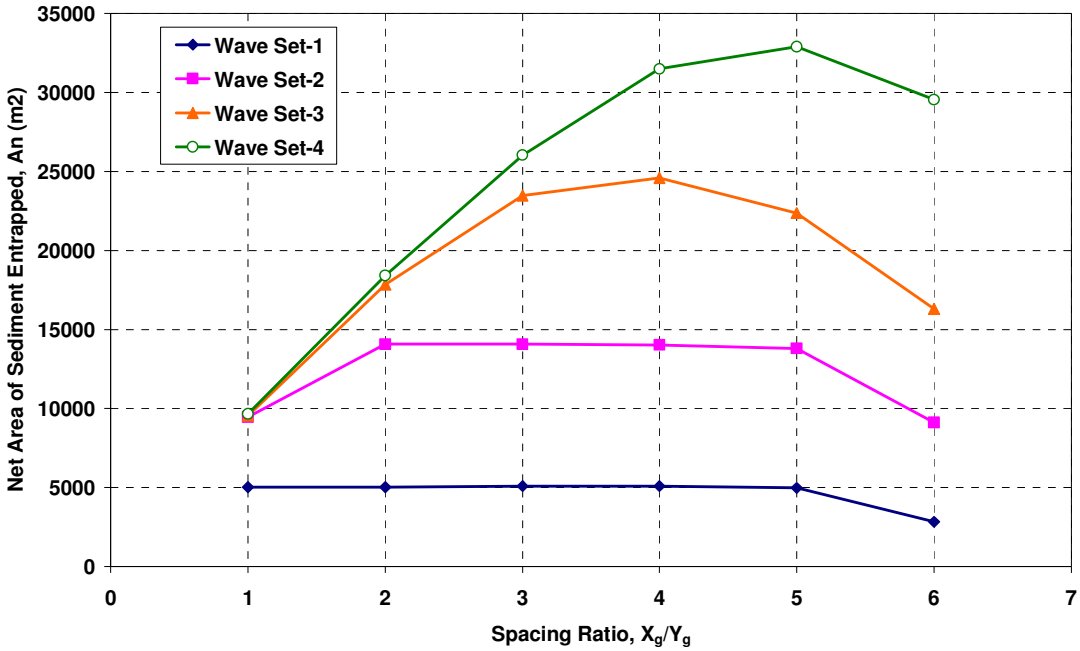

Figure 3.21 Variation of the net area of sediment entrapped

As shown in Figure 3.21, the net area of sediment entrapped in groin compartments increases as the net longshore sediment transport rate increases. For Wave Set-1, the net area (A_n) is minimum compared to other wave sets and spacing seems to have no effect on sediment entrapment capacity. Similarly, for Wave Set-2, the net area remains almost the same for spacing ratios 2.0, 3.0, 4.0 and 5.0 and the maximum capacity is reached for spacing ratio equal to 3.0. However, as the net longshore sediment transport rate increases, spacing ratio becomes effective on the net area of sediment entrapped in groin compartments, that is observed for Wave Set-3 and -4. For these wave sets, spacing ratios 4.0 and 5.0 give maximum net area respectively. Considering entrapment capacity, greater spacing values (4.0-5.0) seem to be better for the functional design of groin fields. However the amounts of erosion in compartments also increases for increasing spacing ratios (see Figure 3.22) due to the facts that groins work more individually and more time is required for compartments to be filled up or to have an equilibrium planform, that can be observed also from the decreases in A_n for spacing ratio , X_g/Y_g = 6.0, for all wave sets.

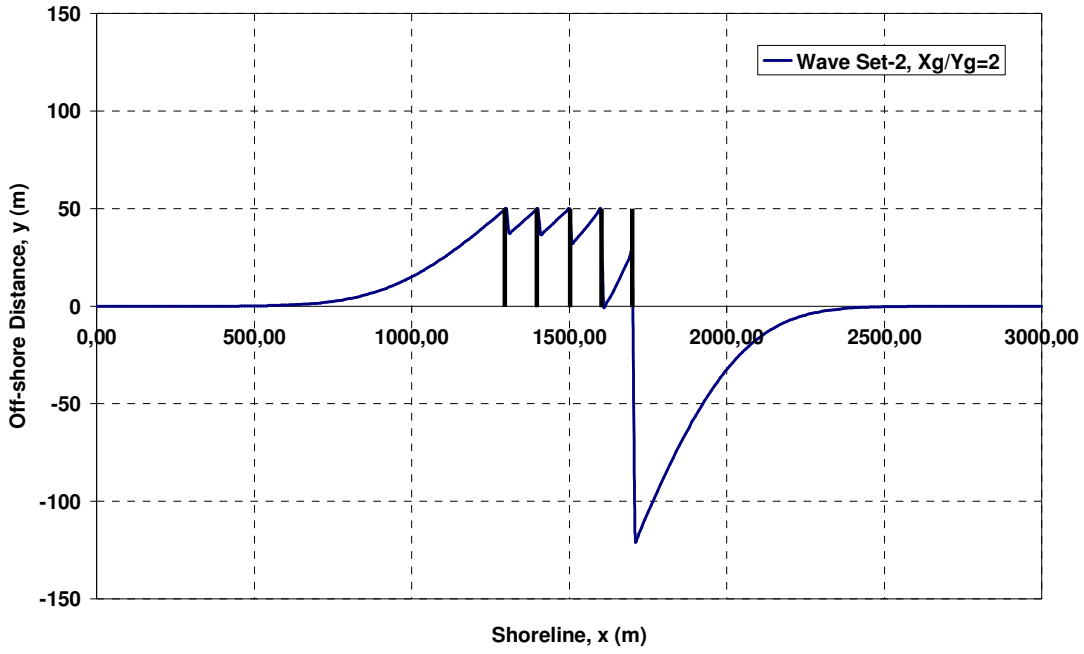

(a)

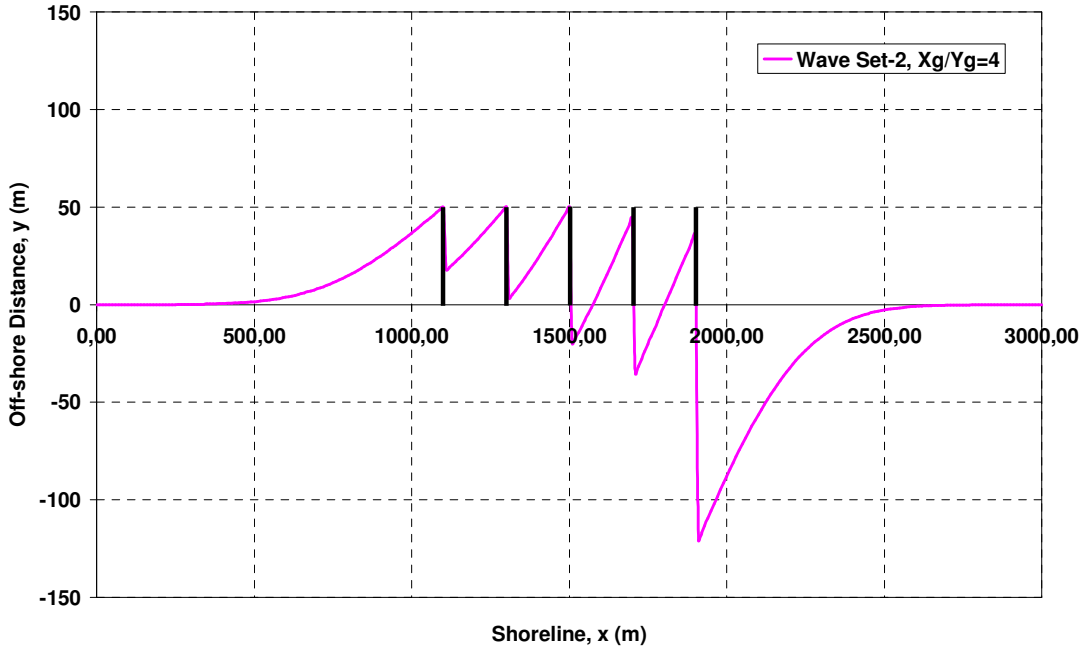

(b)

Figure 3.22 Shoreline positions at the groin field after 5000 hours for wave set

In Figure 3.22, the shoreline positions at the groin field for two spacing ratios (2.0 and 4.0) after 5000 hours simulation with the Wave Set-2 are illustrated. The groin

field for spacing ratio equal to 2.0 starts at 1300 meters on the shoreline and has a spacing of 100 meters (see Figure 3.22.a). For spacing ratio equal to 4.0 (200 meters), the groin field starts at 1100 meters on the shoreline (see Figure 3.22.b). As it can be easily seen from the figure, the amounts of erosion in groin compartments after 5000 hours is greater for the spacing ratio, X_g/Y_g = 4.0, which concludes that the allowable landward limit of erosion is an important parameter to be considered in the functional design of groin fields and a spacing ratio between 2.0 to 3.0 may be applicable for most of the common practices as it is also recommended in literature. Another thing that may be concluded from the results is that the numerical model is able to show the validity of the recommended spacing ratio values.

CHAPTER 4

MODEL BENCHMARKING WITH ANALYTICAL SOLUTIONS

In this chapter, general background information about analytical solutions for shoreline changes, analytical solutions for accretion and erosion (including diffraction) at groins and jetties and comparison of results of these solutions and the numerical model developed are presented.

4.1 BACKGROUND OF ANALYTICAL SOLUTIONS

Mathematical modeling of shoreline change is a powerful and flexible engineering technique for understanding and predicting the long-term evolution of the plan shape of sandy beaches. In particular, mathematical models provide a concise, quantitative means of describing systematic trends in shoreline evolution commonly observed at groins, jetties, and detached breakwaters (Larson et al., 1987).

Qualitative and quantitative understanding of idealized shoreline response to the governing processes is necessary for investigating the response of the beach to engineering actions. By developing analytical or closed-form solutions originating from mathematical models that describe the basic physics involved, essential features of beach response may be derived, isolated, and more readily comprehended than in complex approaches such as numerical and physical modeling. Also, with an analytical solution as a starting point, direct estimates can be readily made of characteristic parameters associated with a phenomenon, such as the time elapsed before bypassing of a groin occurs, percentage of volume lost from a beach fill, and growth of a salient behind a detached breakwater. In addition, analytical models avoid inherent numerical stability and numerical diffusion problems encountered in mathematical models (Larson et al., 1987).

Another useful property of analytic solutions is the capability of obtaining equilibrium condition from asymptotic behavior. However, the complexity of beach change implies that results obtained from an analytic model should be interpreted with care and with awareness of the underlying assumptions. Analytic solutions of mathematical models cannot be expected to provide quantitatively accurate results in situations involving complex boundary conditions and complex wave inputs. In engineering design, a numerical model of shoreline evolution would usually be more appropriate (Larson et al., 1987).

Pelnard-Considere (1956) is the first to employ mathematical modeling as a method of describing shoreline evolution. He introduces the "one-line" theory and verifies its applicability with laboratory experiments of shoreline change at a groin.

Grijm (1961) studies delta formation from rivers discharging sand. The sand transport rate is set to be proportional to twice the incident breaking wave angle to the shoreline, and two different analytical solutions are presented. The governing equations (sand transport and mass conservation) are expressed in polar coordinates and solved numerically. Grijm (1965) further develops this technique and presents solutions for a wide range of delta formations. Komar (1973) also presents numerically obtained solutions of delta growth under simplified conditions.

LeMéhauté and Brebner (1961) discuss solutions for shoreline change at groins, with and without bypassing of sand, and the effect of sudden injection of material at a given point. Bakker and Edelman (1965) modify the longshore sand transport rate equation to allow for an analytical treatment without linearization.

Bakker (1968) extends the "one-line" theory to include two lines describing beach planform change. The beach profile is divided into two parts; one relating to shoreline movement and one relating to the movement of an offshore contour (see Figure 4.1). The two-line theory provides a better description of sand movement downdrift of a long groin because it describes representative changes in the contours seaward of the groin head. The two-line theory is further developed in

Bakker et al. (1971), in which diffraction behind a groin is treated. In this case, it becomes necessary to numerically solve the governing equations.

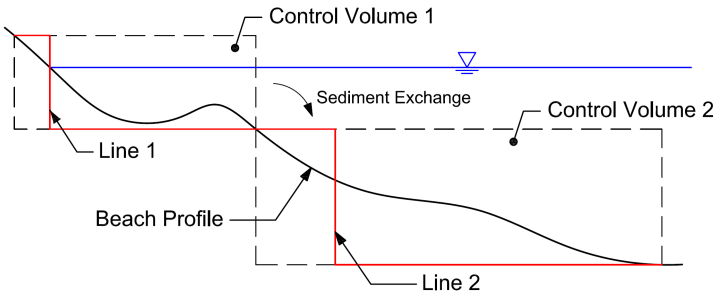

Figure 4.1 The two-line theory (after Bakker 1968)

In LeMéhauté and Soldate (1977), analytical solutions of the linearized shoreline change equation are discussed together with the spread of a rectangular beach fill. LeMéhauté and Soldate (1978; 1979) develop a numerical model that includes variation in sea level, wave refraction and diffraction, rip currents, and the general influence of coastal structures on long-term shoreline evolution.

A summary of analytical solutions of the one-line model is given in Walton and Chiu (1979). Two derivations of the linearized shoreline change equation are presented together with another approach resulting in a nonlinear model. New solutions include beach fill placed in a triangular shape, a rectangular gap in a beach, and a semi-infinite rectangular fill.

Hanson and Larson (1987) present comparisons between analytical and numerical solutions concluding that the inability to include wave refraction in the analytic solution is significantly more restrictive for the applicability of the analytic solution than the small angle approximation.

Dean (1983) gives a short survey of some solutions applicable to beach nourishment calculations, especially in the form of characteristic quantities describing loss percentages.

Larson et al. (1987) review previous solutions and introduce a large number of new solutions. The new solutions are derived either from analogies with heat conduction or through the Laplace transform technique. Solutions describing shoreline change without coastal structures are presented that are applicable both to natural and artificial beach forms. Also, several solutions describing river-delta formation are presented.

Bodge and Kraus (1991) derive values on the diffusion coefficient (ε) for different coastal sites around the United States. The analytical solution for the accumulation updrift a groin or jetty is least-square fitted against the measured shoreline evolution with diffusion coefficient (ε) as the only free parameter (and neglecting bypassing).

Walton (1994) presents an analytical solution for the case of a rectangular beach fill with tapered ends. The loss of fill material with elapsed time is calculated for different beach fill configurations. For comparison, Hanson and Kraus (1993) present numerical solutions for a tapered fill.

4.2 ANALYTICAL SOLUTIONS FOR SHORELINE CHANGES AT GROINS AND JETTIES

The easiest way to test the validity of the numerical model is to compare it with the analytical solutions for cases such where a change in shoreline occurs due to obstacles like groins, jetties and detached breakwaters. However, in order to treat such a case analytically, the situation has to be idealized to a large degree (Larson et al., 1987). The analytical solution for shoreline change at a groin or any thin shore-normal structure is introduced first by Pelnard-Considere (1956). The existence of an equilibrium beach profile, which means that the seafloor is in equilibrium with

average wave conditions, is the major assumption of this solution. A definition sketch for shoreline change at a specific location at any time is given in Figure 4.2.

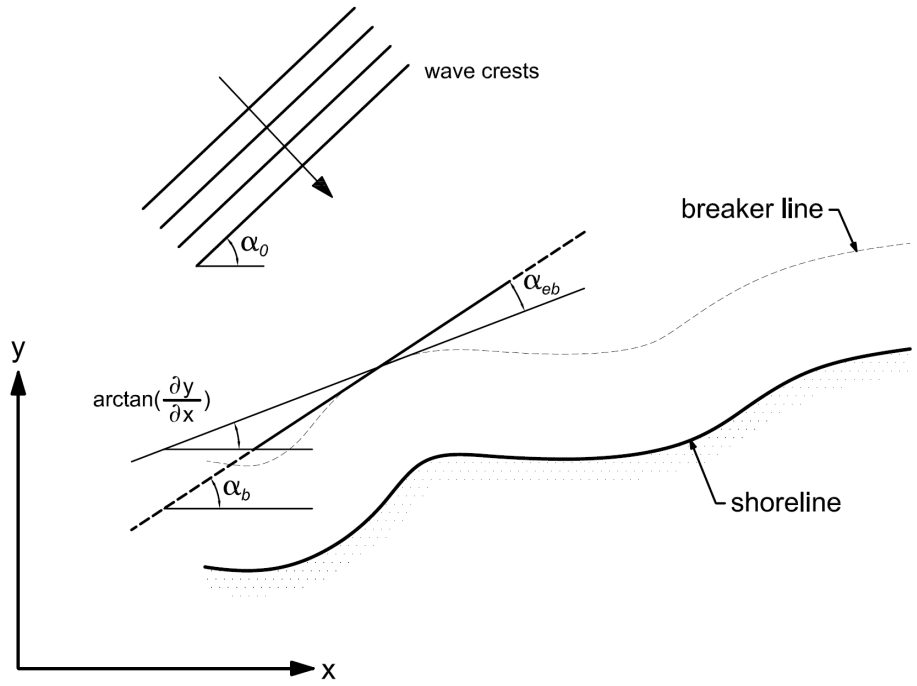

Figure 4.2 Shoreline change at a specific location at any time

The local shoreline orientation with respect to a coordinate system at any time, as shown in Figure 4.2, is $\partial y/\partial x$ and the effective local breaking wave angle (α_{eb}) with respect to the new shoreline is defined as

$$\alpha_{eb} = \alpha_b - \arctan(\frac{\partial y}{\partial x}) \tag{4.1}$$

where α_b is the incident breaking wave angle. A general form of longshore sediment transport rate formula is given in equation (4.2) (Pelnard-Considere, 1956);

$$Q = Q_0 \cdot \sin(2\alpha_b) \tag{4.2}$$

where Q_0 is the amplitude of longshore sediment transport, and substituting equation (4.1) into (4.2), results in

$$Q = Q_0 \cdot \sin\left[2(\alpha_b - \frac{\partial y}{\partial x}) \right] \tag{4.3}$$

For small breaking angles, it can be assumed that

$$\sin(2\alpha_{eb}) \cong 2\alpha_{eb} \tag{4.4}$$

and equation (4.3) becomes

$$Q = Q_0 \cdot \left[2(\alpha_b - \frac{\partial y}{\partial x}) \right] \tag{4.5}$$

If the amplitude of the longshore sand transport rate and the incident breaking wave angle are constant (independent of x and t) and no sources or sinks exists, the following equation may be derived from (3.3) and (4.5)

$$\frac{\partial y}{\partial t} = \varepsilon \frac{\partial^2 y}{\partial x^2} \tag{4.6}$$

where ε is the diffusion coefficient defined as

$$\varepsilon = \frac{2Q_0}{(D_c + B)} \tag{4.7}$$

Since equation (4.6) is formally identical to the one-dimensional equation describing conduction of heat in solids or the diffusion equation, many analytical solutions can be generated by applying the proper analogies between initial and boundary conditions for shoreline evolution and the processes of heat conduction and diffusion (Larson et al., 1987).

4.2.1 Accretion

The analytical solution for accretion at a groin considers an initially straight shoreline (y = 0 along the x-axis) which is in equilibrium with the same incident breaking wave angle (α_b) existing everywhere, thus leading to a uniform sand transport rate along the shoreline. To represent accretion at a complete barrier, a boundary condition given in (4.8) is introduced such that at time t = 0, a thin groin is instantaneously placed at x = 0, blocking all transport (see Figure 4.3).

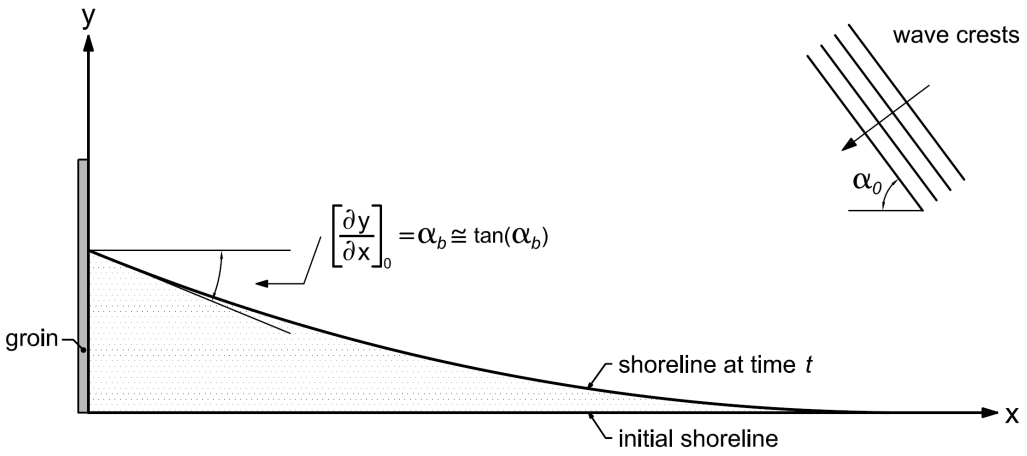

Figure 4.3 Shoreline change at the updrift of a groin

$$Q_0 = 0 \text{ at } x=0 \tag{4.8}$$

Substituting equation (4.8) into (4.5), the following equation is obtained.

$$\left[\frac{\partial y}{\partial x}\right]_0 = \alpha_b \cong \tan(\alpha_b) \text{ at } x=0 \tag{4.9}$$

Equation (4.9) states that the shoreline at the groin is at every instant parallel to the wave crests. The solution for the accretion at a complete barrier is given in Larson et al. (1987) as

$$y(x,t) = 2\tan(\alpha_b) \cdot \sqrt{\varepsilon t} \cdot ierfc(\frac{x}{2\sqrt{\varepsilon t}}) \tag{4.10}$$

where ε is the diffusion coefficient, α_b is the incident breaking wave angle and *ierfc* function is known as the "first integral of complementary error function".

The "error function" (*erf*) is encountered in integrating the normal distribution (which is a normalized form of the Gaussian function). It is an entire function defined as:

$$erf(x) = \frac{2}{\sqrt{\pi}} \cdot \int_0^x e^{-t^2} dt \tag{4.11}$$

The "complementary error function" (*erfc*) and the "first integral of complementary error function" are given in equation (4.12) and (4.13) respectively. The *erf* and *erfc* functions are shown in Figure 4.4.

$$erfc(x) = 1 - erf(x) \tag{4.12}$$

$$ierfc(x) = \frac{1}{\pi} e^{-x^2} - x \cdot erfc(x) \tag{4.13}$$

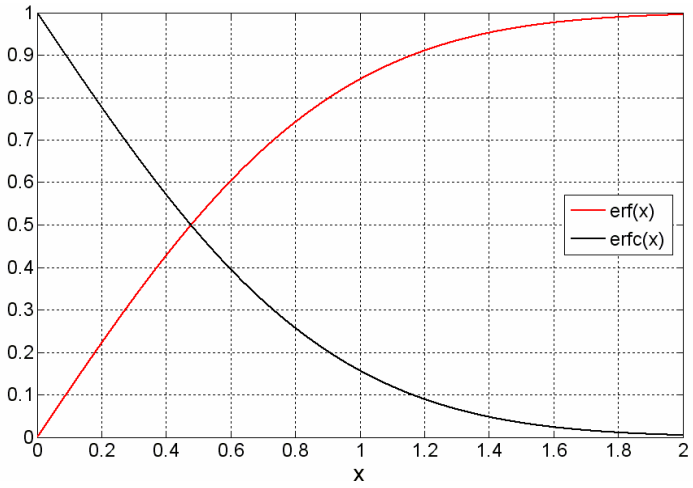

Figure 4.4 Error and complementary error functions

Substituting (4.13) into (4.10) yields

$$y(x,t) = 2\tan(\alpha_b) \cdot \left[\sqrt{\frac{\varepsilon t}{\pi}} \cdot e^{-x^2/4\varepsilon t} - \frac{x}{2} \cdot erfc\left(\frac{x}{2\sqrt{\varepsilon t}}\right) \right] \tag{4.14}$$

where y is the shoreline position at any distance (x) and time (t), ε is the diffusion coefficient, α_b is the incident breaking wave angle and *erfc* function is the complementary error function (4.12).

4.2.2 Erosion (Including Diffraction)

In the shadow region of a long groin or jetty, it may be an oversimplification to neglect the process of wave diffraction. Erosion just behind the jetty will be overestimated if diffraction is neglected because the wave height is assumed to be constant alongshore. Accordingly, by including a variation in wave height (and thus in the amplitude of the sand transport rate) in the shadow region, a more realistic description of shoreline change will be obtained (Larson et al. 1987).

There are a number of ways to account for varying amplitude in the longshore sand transport rate (resulting from varying wave height). One way is to divide the shadow region into distinct solution areas, each having constant amplitude of the sand transport rate. The incident breaking wave angle may also be varied from one solution area to another. Another way is to assume either the amplitude of the longshore sediment transport rate or the incident breaking wave angle as a function of x in the sheltered zone (Larson et al., 1987). A definition sketch for shoreline change at the downdrift of a groin is given in Figure 4.5.

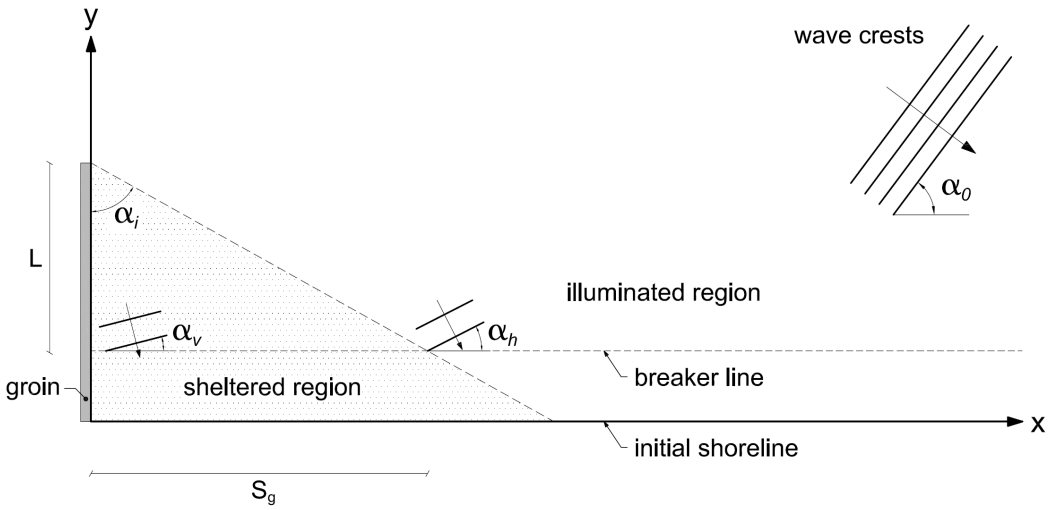

Figure 4.5 Shoreline change at the downdrift of a groin

For the case, in which the incident breaking wave angle is a continuous function of *x*, the governing differential equation for the shoreline (Larson et al., 1987) takes a different form:

$$\frac{\partial^2 y}{\partial x^2} = \frac{1}{\varepsilon}\frac{\partial y}{\partial t} + \frac{d\alpha_b}{dx} \tag{4.15}$$

The variation of the incident breaking wave angle, α_b, is given by equation (4.16);

$$\alpha_b = \alpha_v + (\alpha_h - \alpha_v) \cdot \frac{x}{S_g} \tag{4.16}$$

$$S_g = L \cdot \tan(\alpha_i) \tag{4.17}$$

where α_v is the incident breaking angle at the groin, α_h is the angle in the illuminated region and S_g is the length of sheltered zone on the breaker line, along which breaking wave angle is assumed to be a function of *x*, and is found from equation (4.17). L is the length of groin from breaker line to the seaward tip of groin

and α_i is the incident wave angle at the seaward tip of the groin (see Figure 4.5). The analytical solution for this problem is

$$y(x,t) = \frac{(\alpha_h - \alpha_v)\varepsilon t}{S_g}\left[2 \cdot i^2 erfc(\frac{S_g - x}{2\sqrt{\varepsilon t}}) + 2 \cdot i^2 erfc(\frac{S_g + x}{2\sqrt{\varepsilon t}}) - 1 \right]$$

$$- \tan(\alpha_v)\left[2\sqrt{\frac{\varepsilon t}{\pi}} e^{-x^2/4\varepsilon t} - x \cdot erfc(\frac{x}{2\sqrt{\varepsilon t}}) \right] \qquad (4.18)$$

for $t > 0$ and $0 \le x \le S_g$,

$$y(x,t) = \frac{(\alpha_h - \alpha_v)\varepsilon t}{S_g}\left[2 \cdot i^2 erfc(\frac{x + S_g}{2\sqrt{\varepsilon t}}) - 2 \cdot i^2 erfc(\frac{x - S_g}{2\sqrt{\varepsilon t}}) \right]$$

$$- \tan(\alpha_v)\left[2\sqrt{\frac{\varepsilon t}{\pi}} e^{-x^2/4\varepsilon t} - x \cdot erfc(\frac{x}{2\sqrt{\varepsilon t}}) \right] \qquad (4.19)$$

for $t > 0$ and $x > S_g$, where $i^2erfc(x)$ is the "second integral of complementary error function" given in equation (4.20).

$$i^2 erfc(x) = \frac{1}{4} erfc(x) - \frac{x}{2\sqrt{\pi}} e^{-x^2} + \frac{x^2}{2} erfc(x) \qquad (4.20)$$

Larson et al. (1987) states that the solution obtained for a variable breaking wave angle overestimates the rates of erosion behind the groin since it is assumed that the amplitude of the longshore sand transport rate is the same everywhere (and thus that the wave height, in principle, is constant). In reality, diffraction reduces the wave height in the shadow region and, accordingly, the amplitude of the longshore sand transport rate there (Larson et al., 1987). It is also said in Larson et al. (1987) that despite this reduction, equations (4.18) and (4.19) provide a better description of the

actual situation than the commonly used solution without diffraction for which maximum erosion will always appear immediately adjacent to the groin.

4.2.3 Model Benchmarking with Analytical Solutions

The benchmarking of the numerical model with the analytical solution of accretion and erosion (including diffraction) at a complete barrier is carried out for wave parameters such that deep water significant wave height and period are 1.0 meter and 4.0 seconds respectively as Kamphuis's (1991) longshore sediment transport formula, which gives more consistent predictions for wave height less than 1.0 m (Wang et al., 2002), is used in the model. Considering small breaking wave angle assumption of "one-line" theory, the comparison for accretion is done for breaking wave angles; -2.0, -5.0 and -10.0 degrees resulting sediment transport in negative direction. The expected shoreline changes computed from analytical solution and numerical model after a year have been shown in Figure 4.6.

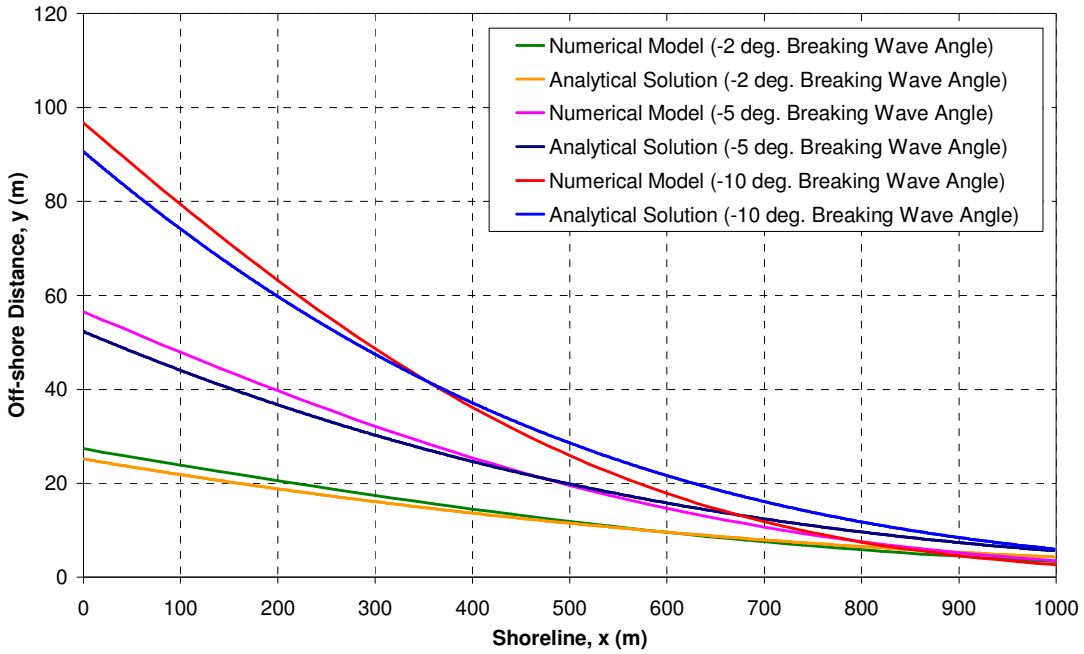

Figure 4.6 Accretion at a groin after a year

As shown in Figure 4.6, the numerical model results match well with the analytical solution results both qualitatively and quantitatively even for large breaking wave angles such as 10.0 degrees.

The benchmarking of the numerical model with the analytical solution of the erosion including diffraction at a complete barrier is carried out for the breaking wave angles given as 2.0, 5.0 and 10.0 degrees resulting a sediment transport in positive direction. The expected shoreline changes computed from analytical solution and numerical model after a year have been shown in Figure 4.7.

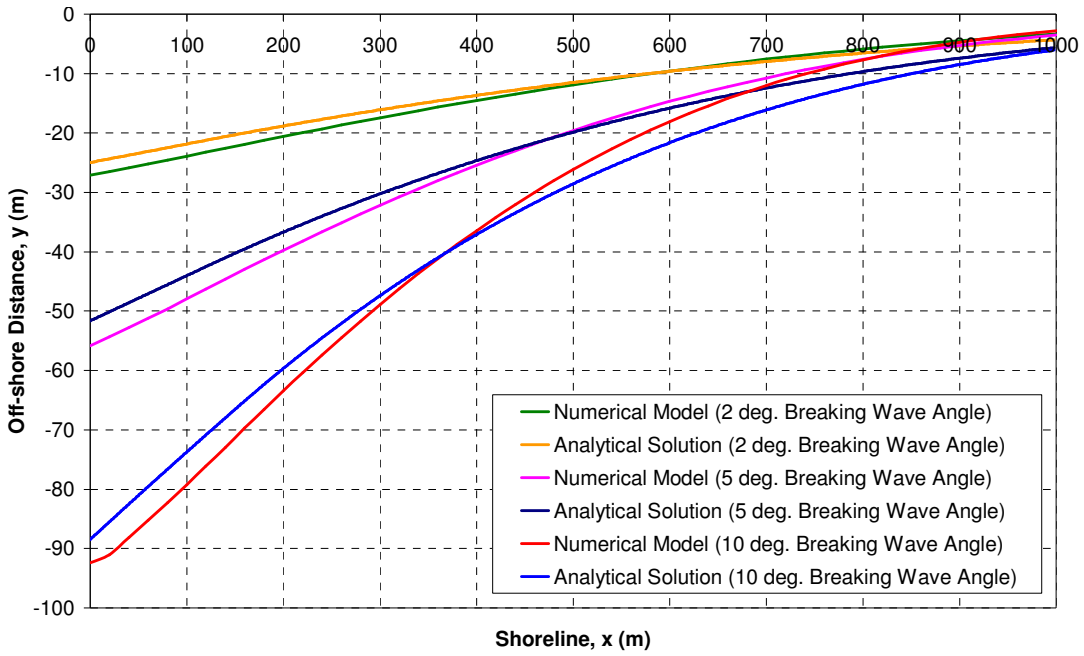

Figure 4.7 Erosion at a groin after a year

As shown in Figure 4.7, the results of the numerical model and analytical solutions for erosion (including diffraction) are in good agreement showing that the assumptions made for calculation of breaking wave parameters in the sheltered zones of shore-normal diffracting coastal structures (groins, jetties etc.) works well enough to match with the analytical solution for erosion.

CHAPTER 5

A CASE STUDY

In this chapter, an application of the numerical model developed to a case study is presented. The model results and field measurements for shoreline changes at a groin field constructed to the east of Kızılırmak river mouth at Bafra alluvial plain are compared.

5.1 INTRODUCTION

Benchmarking a numerical model with analytical solutions is easy and straightforward. The behavior of the model for an idealized case, where less unknown parameters exist, is important to check the numerical and theoretical background of the model. However, in order to be used in engineering and scientific practices, the model should also be tested with actual cases, which is rather a difficult task due to the fact that simplifying the complex natural phenomena with assumptions and mathematical expressions may lead the model give erroneous results.

To test the numerical model with actual field data, an application of the model to case of a groin field in Bafra Delta, where Kızılırmak River discharges into Black Sea (see Figure 5.1), is performed. Due to the construction of flow regulation structures (Altınkaya and Derbent Dams) on Kızılırmak River, the amount of sediment carried to the sea has reduced over years resulting coastal erosion, up to 30 m. per year in the region (Kökpınar et al., 2005). To the east side of the river mouth, a shore protection system consists of 2 Y-shaped groins and 6 I-shaped groins exist (see Figure 5.2). The performance of the first part of the system constructed formerly, 2 Y-shaped groins and I-shaped groin, is studied by Kökpınar et al. (2005) and Şafak (2006). The second part of the system that consists of a

series of 5 groins is used to benchmark the model in this study. Measured field data including shoreline positions between the years 2003-2004 is obtained from State Hydraulic Works (DSİ) to be used in this case study.

Figure 5.1 Location of Bafra alluvial plain

Figure 5.2 Plan view of the existing shore protection system at the Kızılırmak river mouth (Google Earth, 2006)

5.2 WAVE CLIMATE STUDY

Shoreline evolution is the result of a time history of short-term uncorrelated wave events occurring quasirandomly. This time history is rarely available. Instead, a wave hincasting study can be performed to determine the wave climate of the region from available hourly wind data measured by a local meteorological station for years. For each direction, the wind velocities and fetch lengths are used to hindcast the yearly or seasonal deep water wave characteristics of the shoreline and a long-term wave statistics study is carried out to determine annual or seasonal log-linear probability distribution function of deep water significant wave height.

In the wave climate study of the site, wind data measured by Sinop Meteorological Station between the years 1966-1985 is obtained from DMİGM (General Directorate of Meteorological Affairs). The location of the site is open to waves approaching from North-West (NW), North-North-West (NNW), North (N), North-North-East (NNE), North-East (NE), East-North-East (ENE), East (E), and East-South-East (ESE). Further performing a refraction analysis, waves from West-North-West (WNW) direction are also found to be effective at site. The wave directions for Bafra region (see Figure 5.3) and the fetch distances for these directions given by Şafak (2006) are presented in Table 5.1.

Table 5.1 Fetch distances for all directions (Şafak, 2006)

FETCH DISTANCES (km.)	
WNW	617
NW	502
NNW	373
N	330
NNE	331
NE	333
ENE	382
E	349
ESE	282

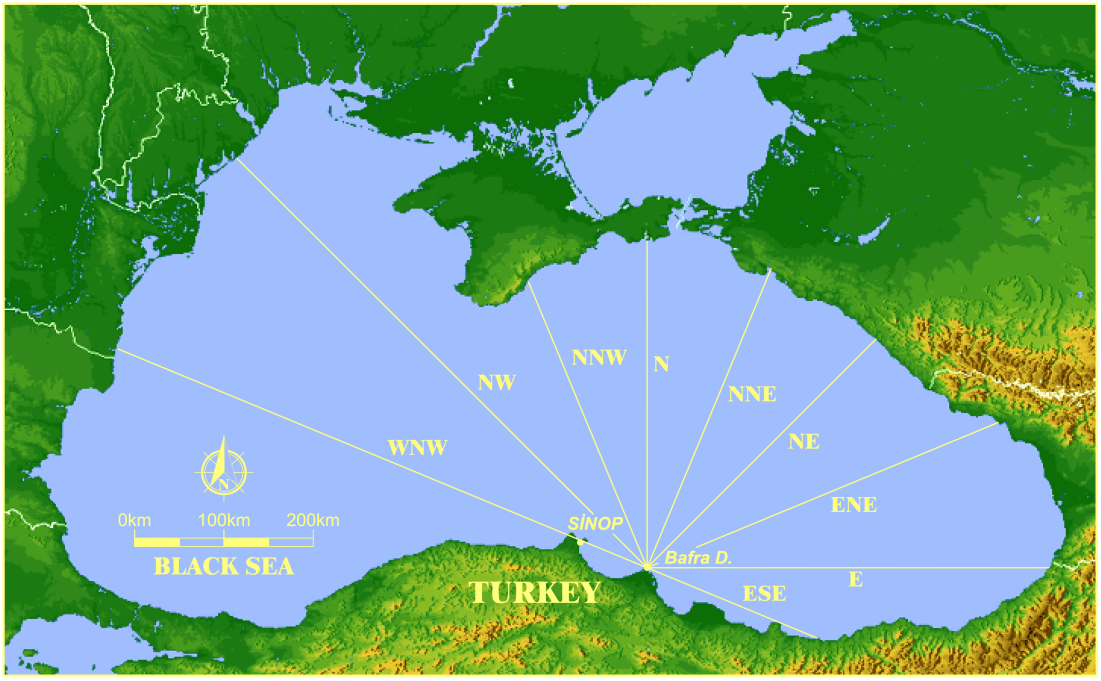

Figure 5.3 Wave directions for Bafra region

Using the 20 year wind data, which contains measured hourly average wind velocities (greater than 3 m/sec as storm condition), and corresponding directions, and the fetch distances for all directions, a history of storm waves are obtained. Since the available shoreline measurements are limited to 1-year, a seasonal based wave data input is assumed to represent the actual wave conditions better, minimizing the effect of wave data sequence discussed in Şafak (2006). To prepare the wave data input for the model, seasonal based long-term wave statistics are carried out and seasonal probability distribution functions of deep water significant wave heights for wave directions are obtained (see Table 5.2 below and Figure A.1).

Table 5.2 Seasonal probability distribution functions of deep water significant wave heights for all directions

(a)

	SPRING
WNW	$(H_{1/3})_0 = -1{,}16415 \cdot \ln[Q(>(H_{1/3})_0)] - 2{,}52560$
NW	$(H_{1/3})_0 = -0{,}67208 \cdot \ln[Q(>(H_{1/3})_0)] - 0{,}67498$
NNW	$(H_{1/3})_0 = -0{,}62682 \cdot \ln[Q(>(H_{1/3})_0)] - 1{,}23558$
N	$(H_{1/3})_0 = -0{,}73463 \cdot \ln[Q(>(H_{1/3})_0)] - 2{,}53321$
NNE	$(H_{1/3})_0 = -0{,}81140 \cdot \ln[Q(>(H_{1/3})_0)] - 3{,}54757$
NE	$(H_{1/3})_0 = -0{,}59711 \cdot \ln[Q(>(H_{1/3})_0)] - 2{,}92491$
ENE	$(H_{1/3})_0 = -0{,}69954 \cdot \ln[Q(>(H_{1/3})_0)] - 3{,}81844$
E	$(H_{1/3})_0 = -0{,}61388 \cdot \ln[Q(>(H_{1/3})_0)] - 2{,}40942$
ESE	$(H_{1/3})_0 = -0{,}89984 \cdot \ln[Q(>(H_{1/3})_0)] - 1{,}65921$

(b)

	SUMMER
WNW	$(H_{1/3})_0 = -0{,}83344 \cdot \ln[Q(>(H_{1/3})_0)] - 0{,}85088$
NW	$(H_{1/3})_0 = -0{,}47994 \cdot \ln[Q(>(H_{1/3})_0)] - 0{,}09014$
NNW	$(H_{1/3})_0 = -1{,}08848 \cdot \ln[Q(>(H_{1/3})_0)] - 2{,}98325$
N	$(H_{1/3})_0 = -0{,}53178 \cdot \ln[Q(>(H_{1/3})_0)] - 1{,}38129$
NNE	$(H_{1/3})_0 = -0{,}54152 \cdot \ln[Q(>(H_{1/3})_0)] - 1{,}55141$
NE	$(H_{1/3})_0 = -0{,}40662 \cdot \ln[Q(>(H_{1/3})_0)] - 1{,}68711$
ENE	$(H_{1/3})_0 = -0{,}32677 \cdot \ln[Q(>(H_{1/3})_0)] - 1{,}17609$
E	$(H_{1/3})_0 = -0{,}63888 \cdot \ln[Q(>(H_{1/3})_0)] - 2{,}69580$
ESE	$(H_{1/3})_0 = -0{,}39799 \cdot \ln[Q(>(H_{1/3})_0)] - 0{,}02891$

Table 5.2 Seasonal probability distribution functions of deep water significant wave heights for all directions (cont'd)

(c)

	AUTUMN
WNW	$(H_{1/3})_0 = -0{,}91052 \cdot \ln[Q(>(H_{1/3})_0)] - 1{,}50401$
NW	$(H_{1/3})_0 = -0{,}91534 \cdot \ln[Q(>(H_{1/3})_0)] - 2{,}02811$
NNW	$(H_{1/3})_0 = -0{,}67122 \cdot \ln[Q(>(H_{1/3})_0)] - 1{,}02061$
N	$(H_{1/3})_0 = -0{,}50100 \cdot \ln[Q(>(H_{1/3})_0)] - 1{,}11103$
NNE	$(H_{1/3})_0 = -0{,}70440 \cdot \ln[Q(>(H_{1/3})_0)] - 2{,}44382$
NE	$(H_{1/3})_0 = -0{,}69852 \cdot \ln[Q(>(H_{1/3})_0)] - 2{,}62370$
ENE	$(H_{1/3})_0 = -0{,}85805 \cdot \ln[Q(>(H_{1/3})_0)] - 3{,}44642$
E	$(H_{1/3})_0 = -0{,}49856 \cdot \ln[Q(>(H_{1/3})_0)] - 1{,}64814$
ESE	$(H_{1/3})_0 = -0{,}35914 \cdot \ln[Q(>(H_{1/3})_0)] - 0{,}13706$

(d)

	WINTER
WNW	$(H_{1/3})_0 = -1{,}30946 \cdot \ln[Q(>(H_{1/3})_0)] - 2{,}79346$
NW	$(H_{1/3})_0 = -0{,}93719 \cdot \ln[Q(>(H_{1/3})_0)] - 1{,}35410$
NNW	$(H_{1/3})_0 = -0{,}95615 \cdot \ln[Q(>(H_{1/3})_0)] - 1{,}89742$
N	$(H_{1/3})_0 = -0{,}62741 \cdot \ln[Q(>(H_{1/3})_0)] - 1{,}69882$
NNE	$(H_{1/3})_0 = -1{,}00414 \cdot \ln[Q(>(H_{1/3})_0)] - 3{,}93210$
NE	$(H_{1/3})_0 = -0{,}74371 \cdot \ln[Q(>(H_{1/3})_0)] - 2{,}97941$
ENE	$(H_{1/3})_0 = -0{,}59101 \cdot \ln[Q(>(H_{1/3})_0)] - 2{,}29947$
E	$(H_{1/3})_0 = -0{,}84345 \cdot \ln[Q(>(H_{1/3})_0)] - 3{,}88403$
ESE	$(H_{1/3})_0 = -1{,}01960 \cdot \ln[Q(>(H_{1/3})_0)] - 2{,}65864$

One major assumption in the preparation of wave data input is such that the effects of smaller but more frequent waves are considered to be more appropriate to use rather than higher waves with less frequency. To check the validity of this

assumption, in this respect, a concept of average wave height based on a probabilistic approach is developed.

By using the long-term statistics in seasonal time scale, the average deep water significant heights (H_{sa}) of waves coming from every direction, their periods and seasonal frequencies in hours for each season are calculated as (Güler, 1997; Güler et al., 1998 and Şafak, 2006);

$$H_{sa} = \frac{\sum (P_i \cdot H_i)}{\sum P_i} \tag{5.1}$$

where H_i is the wave height and P_i is the occurrence probability of wave with height H_i. Occurrence probability (P_i) of wave with height (H_i) is computed by using the corresponding frequencies within the given range as follows;

$$P_i = Q(H_i - k) - Q(H_i + k) \tag{5.2}$$

where Q is the exceedence probability and k is an assigned range to compute occurrence probability.

Average deep water wave steepness in Bafra region is calculated as 0.042 from extreme wave statistics (Şafak, 2006), which is consistent with the value given in Ergin and Özhan (1986) and thus, significant wave period for a given average deep water significant wave height (H_{sa}) is calculated as:

$$T = 3.91 \cdot \sqrt{H_{sa}} \tag{5.3}$$

In Table 5.3, the seasonal wave data input for the model consisting of average wave heights, corresponding periods and seasonal frequencies from all directions is presented.

Table 5.3 Average wave heights, corresponding periods and seasonal frequencies from all directions for each season

	SPRING			SUMMER			AUTUMN			WINTER		
	H_{sa} (m)	T (sec)	f (hrs)	H_{sa} (m)	T (sec)	f (hrs)	H_{sa} (m)	T (sec)	f (hrs)	H_{sa} (m)	T (sec)	f (hrs)
WNW	1.63	5.00	246	1.31	4.47	657	1.38	4.60	368	1.78	5.21	267
NW	1.15	4.20	577	0.97	3.86	1393	1.39	4.61	210	1.41	4.64	459
NNW	1.11	4.12	208	1.56	4.88	135	1.15	4.20	344	1.43	4.67	271
N	1.21	4.31	53	1.02	3.95	96	0.99	3.89	132	1.11	4.12	100
NNE	1.29	4.43	23	1.03	3.97	75	1.18	4.25	51	1.47	4.75	40
NE	1.08	4.06	11	0.91	3.72	15	1.18	4.24	38	1.22	4.32	31
ENE	1.18	4.24	7	0.84	3.58	18	1.33	4.51	33	1.08	4.06	29
E	1.10	4.10	29	1.12	4.14	22	0.99	3.89	44	1.32	4.49	18
ESE	1.37	4.58	301	0.90	3.71	851	0.87	3.64	1153	1.49	4.77	150

5.3 MODELLING OF SITE

The groin field constructed in addition to the first part is modeled starting from Groin-3 to Groin-8 with 200 meter spacing between adjacent groins (see Figure 5.4) on a discretized shoreline that was measured in 2003 by State Hydraulic Works, (DSİ). From the physical analysis of the sediment samples taken from the site, the median grain size diameter (D_{50}) is determined as 0.23 millimeters (Kökpınar et al., 2005). The berm height (B), the landward end of the active profile, is assumed as 2 meters. Starting from Groin-3, the apparent lengths of the groins are given as 175, 195, 200, 200, 180 and 175 meters respectively. It is assumed that no source or sink exists in the application of numerical modeling for the case in Bafra region. The sequence of wave data input (see Table 5.3) in the simulation starts with spring waves from WNW to ESE directions and continues with summer, autumn and winter waves.

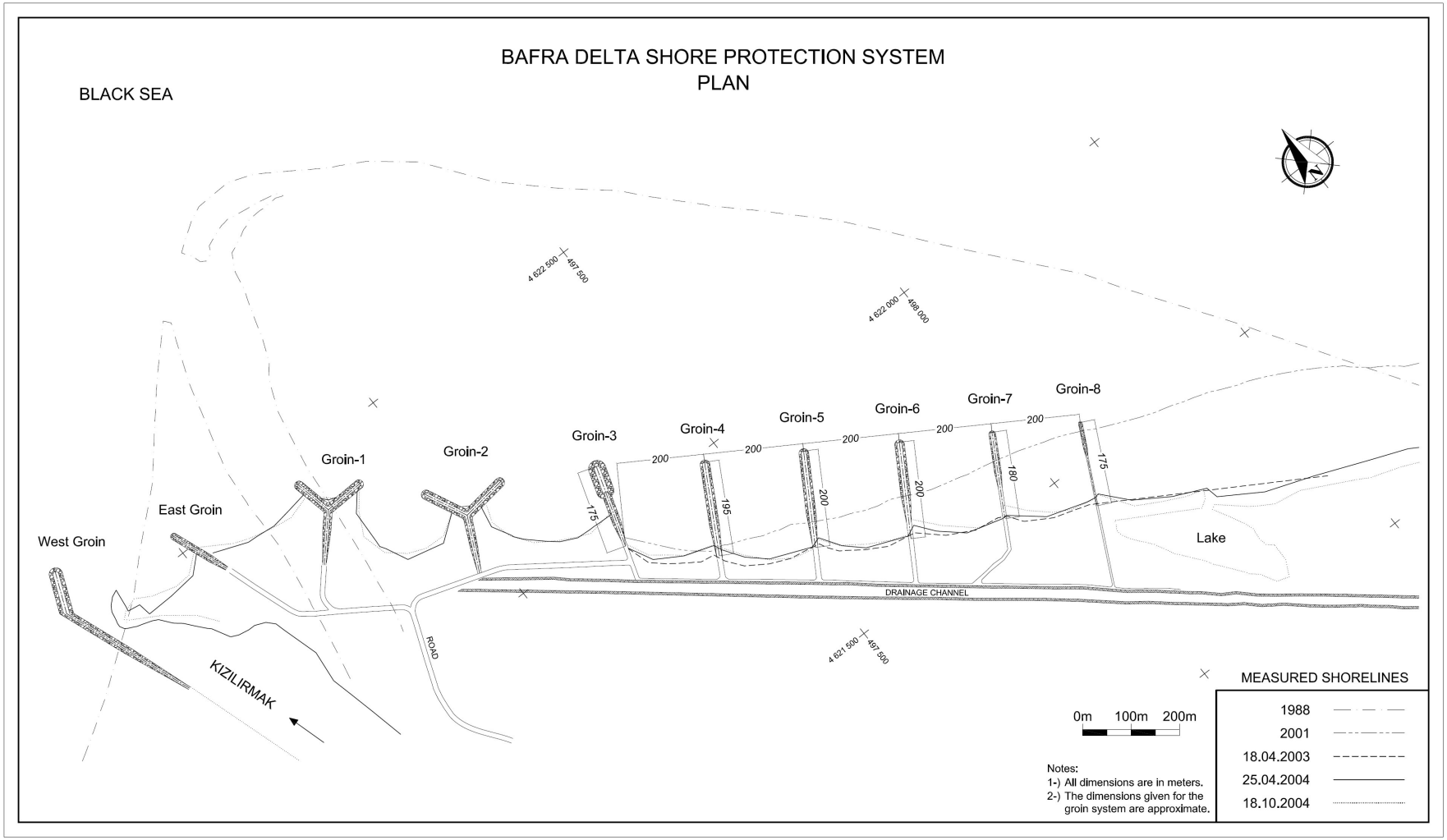

Figure 5.4 Bafra delta shore protection system plan

5.4 RESULTS

The change in shoreline position computed by the numerical model after 1 year simulation time, the off-shore positions of seasonal average limiting depths of longshore sediment transport ($D_{LT,season*}$) and the measured shoreline positions in years 2003 and 2004 representing initial and final shoreline positions respectively are presented in Figure 5.5.

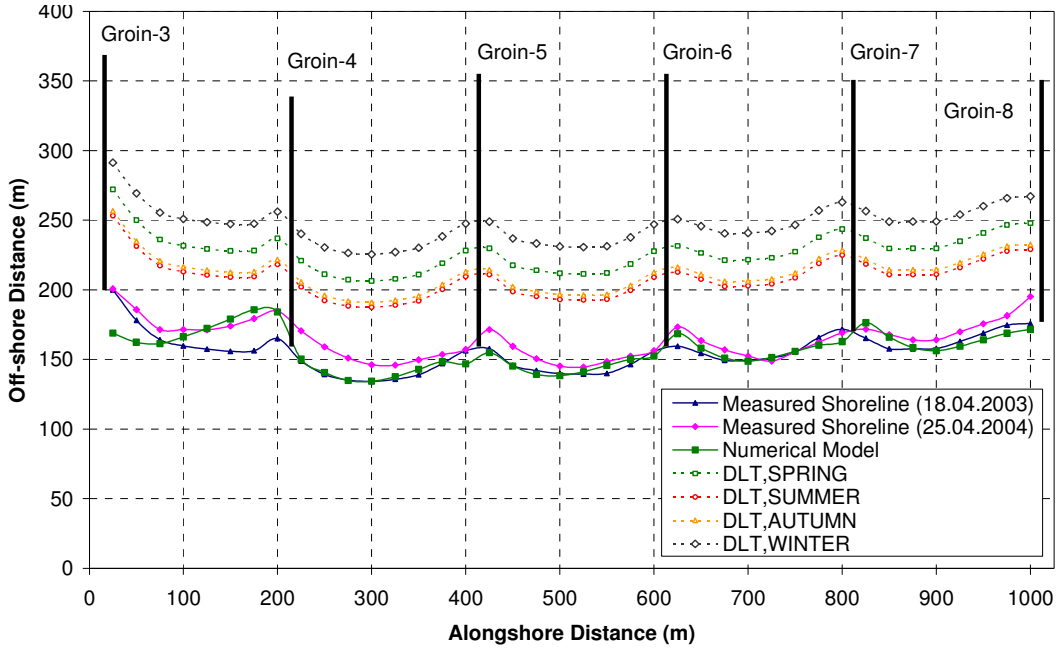

Figure 5.5 Comparison of the site measurements with the numerical simulation

As shown in Figure 5.5, the shoreline change at the groin field computed by the numerical model after a simulation time of 1 year matches well with the shoreline position measured in 2004 qualitatively in general and quantitatively at some locations. Although the general trend in shoreline change is reflected in the model result, quantitatively, there are some differences between the result and field measurement which may be due to many reasons in such a complex and dynamic coastal region where, as stated in Kökpınar et al. (2005), an approximately 1-km-wide band of shoreline has eroded since 1988 (see Figure 5.4). The sequence of

wave data input which is discussed in Şafak (2006), the bottom profile shape assumption, used methodologies in wave climate and transformation studies are all effective parameters in numerical modeling of shoreline evaluation and might be responsible for quantitative disagreement between the measured and computed shoreline positions at some locations of site. During the simulation, the limiting depth of longshore sediment transport for each wave direction of the season is observed to be smaller than the depth of seaward tips of the structures concluding that negligible amount of sediment bypassing around structures happens.

CHAPTER 6

CONCLUSION

The recent studies show that promising results are being achieved with complex three-dimensional models as the computer technology advances and the knowledge about coastal hydrodynamics increases. There are already many available software packages capable of modeling complex problems and tested in many site applications. However, for simpler cases or the cases with not enough available input data, numerical models based on “one-line” theory are still the most effective and easiest to apply to both idealized and actual cases.

Numerical modeling of complex physical phenomena involves assumptions depending on available knowledge and source. Every assumption may ease the problem to be handled, meanwhile it may limit the capabilities of the model or decrease the accuracy of the solution. Numerical models based on “one-line” theory, which include many assumptions and limitations, are generally utilized to achieve qualitative results at first glance. However, the capability of these models to present a qualitative reflection of shoreline changes even for complex actual cases have inspired many other complex modeling techniques. In this respect, the numerical model developed is based on “one-line” theory. Further discussions on the representation of physical coastal processes (e.g., wave transformation, longshore sediment transport mechanism) are made to achieve a generalized and powerful engineering tool.

In the numerical model, an explicit scheme is utilized due to its easiness while defining boundary conditions and constraints, yet, in order to increase the stability and accuracy of the model, an implicit scheme is recommended. For the estimation of deep water waves from measured wind data, a concept of average wave height based on a probabilistic approach is developed. The transformation of deep water

waves to breaking waves is carried out by a wave transformation module in the numerical model which computes breaking wave parameters considering also the effects of diffraction in the sheltered zones of the structures. Shoreline changes are assumed to be due to longshore sediment transport only and hence, a limiting depth of longshore sediment transport as the seaward end of the active profile is defined respectively.

In this study, special emphasis is given on to wave diffraction phenomenon within the sheltered zones of coastal structures while developing a numerical model based on previous studies of one-dimensional models. Available approaches for the computation of the diffracted wave breaking heights within the sheltered zone of a single groin are compared and a simpler approach, which is also more compatible with the theory of "one-line", is followed to describe irregular wave diffraction in the model. Furthermore, for the computation of the diffracted breaking wave angles, a combined refraction-diffraction methodology introduced by Kamphuis (2000) is followed.

The model is benchmarked with both analytical solutions and actual field data. The results of the comparison of the model with the analytical solutions of accretion and erosion (including diffraction) shows that the model gives both qualitatively and quantitatively consistent results with the analytical solutions for some idealized cases. The application of the model in the case study at Bafra Delta proves that the model result and field measurement are in good agreement qualitatively in general and quantitatively at some locations.

In conclusion, considering the limitations and capabilities of shoreline change models based on "one-line" theory, it can be said that the numerical model developed is found to be applicable to actual field cases and it should be tested with several more case studies or laboratory experiments for further calibration and verification of the model as a future recommendation.

REFERENCES

Artagan, S.S., (2006), “A One Line Numerical Model for Shoreline Evolution under the Interaction of Wind Waves and Offshore Breakwaters”, M.S. Thesis, METU, Ankara

Bakker, W.T., (1968), “The Dynamics of a Coast with a Groin System”, Proc. 11th Int. Conf. on Coastal Engrg., ASCE, London, pg.492-517

Bakker, W.T., and Edelman, T., (1965), "The coastline of river deltas." Proc. 9th Int. Conf. on Coastal Engrg., ASCE, New York, pg.199-218

Bakker, W.T., Klein-Breteler, E.H.J., and Roos, A. (1971). "The dynamics of a coast with a groin system." Proc, 12th Int. Conf. on Coast. Engrg., ASCE, New York, pg.1001-1020

Berkhoff, J.C.W., (1972), “Computation of Combined Refraction/Diffraction”, Proc. 13th Int. Conf. on Coastal Engrg., ASCE, Vancouver

Bijker, E.W., (1971), “Longshore Transport Computations”, Journal of Waterways, Harbors and Coastal Engineering Division, ASCE, Vol.97, pg.687-701

Bodge, K.R., and Kraus, N.C., (1991), "Critical examination of long-shore transport rate magnitude" Proc, Coast. Sediment '91, ASCE, New York, pg.139-155.

Briand, M.H.G., and Kamphuis, J.W., (1993), “Sediment transport in the surf zone: A quasi 3-D numerical model”, Coastal Engineering, Vol.20, pg.135-156

Broker-Hedegaard, I., Deigaard, R., and Fredsoe, J., (1991), “Onshore/Off-shore Sediment Transport and morphological Modeling of Coastal Profiles”, Proc. ASCE Special Conf. Coastal Sediment’91, pg.643-657

Bruun, P., (1952), "Measures Against Erosion at Groins and Jetties", Proc. 3rd Conf. on Coastal Engrg., ASCE, Cambridge, Massachusetts, pg.137-164

Capobianco, M., Hanson, H., Larson, M., Steetzel, H., Stive, M.J.F., Chatelus, Y., Aarninkhof, S., Karambas, T., (2002), “Nourishment design and evaluation: applicability of model concepts”, Coastal Engineering, Vol.47, pg.113-135

Coastal Engineering Manual, “CEM” (2003), U.S. Army Corps of Engineers, Coastal Engineering Research Center, U.S.Government Printing Office

Cowell, P., Roy, P.S., Jones, R.A., (1994), “Simulation of LSCB using a morphological behavior model”, Marine Geology, 126, pg.45-61

Dabees, M.A., (2000), “Efficient Modeling of Beach Evolution”, Ph.D. Thesis, Queen’s University, Kingston, Ontario, Canada

Dabees, M.A. and Kamphuis, J.W., (1998), “ONELINE, a Numerical Model for Shoreline Change”, Proc. 27th Int. Conf. On Coastal Engrg., ASCE, Copenhagen, pg.2668-2681

Dally, W.R., and Dean, R.G., (1984), “Suspended Sediment Transport and Beach Profile Evolution”, Journal of Waterways, Harbors and Coastal Engineering Division, ASCE, Vol.110, No.1, pg.15-33

Davies, A.G., van Rijn, A.G., Damgaard, J.S., van de Graaff, J., Ribberink, J.S., (2002), “Intercomparison of research and practical sand transport models”, Coastal Engineering, 46, pg.1-23

Dean, R.G., (1983), CRC handbook of coastal processes and erosion, P.D. Komar, ed., CRC Press, Inc., Boca Raton, Fla.

Dean, R.G., (1991), “Equilibrium Beach Profiles: Characteristics and Applications”, Journal of Coastal Research, Vol.7, No.1, pg.53-84

De Vriend, H.J., Zyserman, J., Nicolson, J., Pechon, P., and Southgate H.N., (1993), “Medium-term 2DH Coastal Area Modelling”, Coastal Engineering, 21, pg.193-224

Ergin, A., and Özhan, E., (1986), “15 Deniz Yöresi için Dalga Tahminleri ve Tasarım Dalgası Özelliklerinin Belirlenmesi” (in Turkish), Middle East Technical University, Ocean Engineering Research Center

Fleming, C.A. and Hunt, J.N., (1976), “Application of a sediment transport model”, Proc. 15th Int. Conf. on Coastal Engrg., ASCE, pg.1184-1202

Güler, I., (1997), “Investigation on Protection of Manavgat River Mouth”, Yüksel Proje International Co. Inc., Research Project Report

Güler, I., Ergin, A., and Yalçıner, A.C., (1998), “The Effect of the Use of Wave Data for the Numerical Solution of Shoreline Evolution”, Journal of Coastal Research, Special Issue No.26, pg. 195-200

Goda, Y., (1985), “Random Seas and Design of Maritime Structures”, University of Tokyo Press

Goda, Y., Takayama, T., and Suzuki, Y., (1978), “Diffraction Diagrams for Directional Random Waves,” Proc. 16th Int. Conf. on Coastal Engrg., ASCE, pg.628-650.

Grijm, W., (1965), "Theoretical forms of shoreline" Proc. 9th Int. Conf. on Coastal Engrg., ASCE, New York, pg.219-235

Hallermeier, R.J., (1978), “Uses for a Calculated Limit Depth to Beach Erosion”, Proc. 16th Int. Conf. on Coastal Engrg., ASCE, New York, pg.1493-1512

Hanson, H., (1987), “GENESIS: A Generalized Shoreline Change Numerical Model for Engineering Use”, Ph.D. Thesis, University of Lund, Lund, Sweden

Hanson, H., Kraus, N.C., (1986a), “Seawall Boundary Condition in Numerical Models of Shoreline Evolution”, Technical Report CERC-86-3, U.S. Army Engineer Waterways Experiment Station, Vicksburg, MS.

Hanson, H., and Kraus, N.C., (1986b), “Seawall Constraint in Shoreline Numerical Model”, Journal of Waterway, Port, Coastal and Ocean Engineering, Vol.111, No.6, pg.1079-1083

Hanson, H., Kraus, N.C., (1991), “Numerical Simulation of Shoreline Change at Lorain, Ohio”, Journal of Waterway, Port, Coastal and Ocean Engineering, Vol.117, No.1, pg.1-18

Hanson, H., and Kraus, N.C., (1993), "Optimization of beach fill transitions" Beach Nourishment engineering and management considerations, Proc. Coastal Zone '93, D. K. Stauble and N. C. Kraus, eds.,ASCE, New York, pg.103-117

Hanson, H., Aarninkhof, S., Capobianco, M., Jimenez, J.A., Larson, M., Nicholls, R.J., Plant, N.G., Southgate, H.N., Steetzel, H.J., Stive, M.J.F., de Vriend, H.J., (2003), “Modelling of Coastal Evolution on Yearly to Decadal Time Scales”, Journal of Coastal Research, Vol.19, No.4, pg.790-811

Hudson, R. Y., Herrmann, F. A., Sager, R. A., Whalin, R. W., Keulegan, G. H., Chatham, C. E., and Hales, L. Z., (1979), “Coastal Hydraulic Models” Special Report No. 5, U.S. Army Engineer Waterways Experiment Station, Vicksburg, MS.

Jayakumar and Mahadevan R., (1993), “Numerical Simulation of Shoreline Evolution Using a One Line Model”, Journal of Coastal Research, Vol.9, No.4, pg.915-923

Kamphuis, J.W., (1990), “Influence of sand or gravel on the erosion of cohesive sediment”, Journal of Hydraulic Research, Vol.28, No.1, pg.43-53

Kamphuis, J.W., (1991), “Alongshore Sediment Transport Rate”, Journal of Waterway, Port, Coastal and Ocean Engineering, ASCE, Vol.117, pg.624-640

Kamphuis, J.W., (2000), “Introduction to Coastal Engineering and Management”, World Scientific

Kökpınar, M.A., Darama, Y., Güler, I., (2005), “Physical and Numerical Modeling of Shoreline Evaluation of the Kızılırmak River Mouth, Turkey”, Journal of Coastal Research, Vol.21 (in print)

Komar, P.D., (1977), “Beach Sand Transport: Distribution and Total Drift”, Journal of Waterway, Port, Coastal and Ocean Engineering, ASCE, Vol.103 (WW2), pg.225-239

Kraus, N.C., (1984), “Estimate of Breaking Wave Height Behind Structures”, Journal of Waterway, Port, Coastal and Ocean Engineering, ASCE, Vol.110, No. 2, pg.276-282

Kraus, N.C., Gingerich, K.J., and Rosati, J.D., (1989), “DUCK85 Surf Zone Sand Transport Experiment” Technical Report, CERC-89-5, U.S. Army Engineer Waterways Experiment Station, Vicksburg, MS.

Kressner, B., (1928), "Tests with Scale Models to Determine the Effect of Currents and Breakers upon a Sandy Beach, and the Advantageous Installation of Groins” The Technical High School of the Free City of Danzig, Construction Methods, Vol.25, Berlin

Kriebel, D.L. and Dean, R.G., (1984), “Beach and Dune Response to Severe Storms”, Proc. 19th Int. Conf on Coastal Engrg., ASCE, pg.1584-1599

Larson, M. and Kraus, N.C., (1989), “SBEACH: Numerical Model for Simulating Storm Induced Beach Change”, Technical Report CERC-89-9, Department of the Army, Waterways Experiment Station Corps of Engineers, Vicksburg, Mississippi

Larson, M., Hanson, H., Kraus, N.C., (1987), “Analytical solutions of the one-line model of shoreline change”, Technical Report CERC-87-15, Department of the Army, Waterways Experiment Station Corps of Engineers, Vicksburg, Mississippi

Larson, M., Hanson, H., Kraus, N.C., (1997), “Analytical solutions of one-line model for shoreline change near coastal structures”, Journal of Waterway, Coastal and Ocean Engineering, Vol.123, No. 4, pg.180-191

LeMéhauté, B., and Brebner, A., (1961), "An introduction to coastal morphology and littoral processes", Rep.No.14, Civil Engrg. Dept., Queens Univ. at Kingston, Ont., Canada

LeMéhauté, B., and Soldate, M., (1978) “Mathematical modeling of shoreline evolution”, Proc. 16th Int. Conf. on Coastal Engrg., ASCE, pg.1163-1179

Leont’yev, I.O., (1999), “Modelling of morphological changes due to coastal structures”, Coastal Engineering, Vol.38, pg.143–166

LITPACK 2004, LITLINE User Guide, DHI (Danish Hydraulics Institute)

Liu, P.L-F., (1982), “Combined Refraction and Diffraction: Comparison Between Theory and Experiments”, Journal of Geophysical Research, Vol.87, No.C8, pg.5723-5730

Liu, P.L-F., and Lozano, C., (1979), "Combined Wave Refraction and Diffraction", Proc. Coastal Structures'79 Conf., ASCE, pg.978-997

Miller, J.K. and Dean R.G., (2004), "A simple new shoreline change model", Coastal Engineering, Vol.51, pg.531-556

Pelnard-Considere, R., (1956), "Essai de Theorie de l'Evolution des Forms de Rivage en Plage de Sable et de Galets", 4th Journees de l'Hydraulique, Les Energies de la Mer, Question III, Rapport No.1, pg.289-298

Penny, W.G., and Price, A.T., (1952), "The Diffraction Theory of Sea Waves by Breakwaters, and the Shelter Afforded by Breakwaters," Philosophical Transactions, Royal Society of London, Series A, Vol.244, pg.236-253

Perlin, M., and Dean, R.G., (1978), "Prediction of Beach Planforms with littoral Controls", Proc. 16th Int. Conf. on Coastal Engrg., ASCE

Pechon, P., and Teisson, C., (1996), "Numerical Modeling of Bed Evolution Behind a Detached Breakwater", Proc. 25th Int. Conf. on Coastal Engrg., ASCE

Price, W.A., Tomlinson, D.W., and Willis, D.H., (1973), "Predicting Changes in the Plan Shape of Beaches", Proc. 13th Int. Conf. on Coastal Engrg., ASCE

Radder, A.C., (1979), "On the Parabolic Equation Method for Water wave Propagation", Journal of Fluid Mechanics, Vol.95, pg.159-176

Reniers, A., Symonds, G., Thornton, E., (2001), "Modelling of rip currents during RDEX", Proc., 4th Coastal Dynamics Conf., Lund, Sweden, pg.493-499

Roelvink, J.A., and Broker, I., (1993), "Cross-shore profile models", Coastal Engineering, Vol. 21, pg.163-191

Roelvink, J.A., Meijer, Th.J., Houwman, K., Bakker, R., and Spanhoff, R., (1995), "Field validation and application of a coastal profile model", Proc. Coastal Dynamics'95, ASCE, pg.818-828

Şafak, I., (2006), "Numerical Modeling of Wind Wave Induced Longshore Sediment Transport", M.S. Thesis, METU, Ankara

Stive, M.J.F. and Battjes, J.A., (1984), "A Model for Offshore Sediment Transport", Proc. 19th Int. Conf. On Coastal Engrg., ASCE, pg.1420-1436

Shore Protection Manual (SPM), (1984), U.S. Government Printing Office, Washington D.C.

Sommerfeld, A., (1896), "Mathematische Theorie der Diffraction," Mathematische Annalen, Vol.47, pg.317-374

Southgate, H.N., (1995), “The effects of wave chronology on medium and long term coastal morphology”, Coastal Engineering, Vol.26, pg.251-270

Swart, D.H., (1975) “Offshore Sediment Transport and Equilibrium Profiles”, PhD Thesis, Delft University of Technology, Delft.

Uda, T., Yamamoto, Y., Itabashi, N., and Yamaji, K., (1996), “Field Observation of Movement of Sand Body Due to Waves and Verification of its Mechanism by a Numerical Model”, Proc. 25th Int. Conf on Coastal Engrg., ASCE

Uda, T., Yamamoto, Y., Itabashi, N., and Yamaji, K., (1998), “Predictive Model of Three-Dimensional Development and Deformation of a River Delta by Applying Contour Line Change Model”, Proc. 26th Int. Conf on Coastal Engrg., ASCE

Van Rijn, L.C., Walstra, D.J.R., Grasmeijer, B., Sutherland, J., Pan, S., Sierra, J.P., (2003), “The predictability of cross-shore bed evolution of sandy beaches at the time scale of storms and seasons using process-based profile models”, Coastal Engineering, Vol.47, pg.295-327

Walton, T. L., (1994), "Shoreline solution for tapered beach fill." Journal of Waterway, Port, Coastal and Ocean Engineering, ASCE, Vol.120, No.6, pg.651-655

Walton, T., and Chiu, T., (1979), "A review of analytical techniques to solve the sand transport equation and some simplified solutions" Proc, Coast. Struc.'79, ASCE, New York, pg.809-837

Wang, P., Ebersole, B.A., and Smith, E.R., (2002), “Longshore Sediment Transport – Initial Results from Large Scale Sediment Transport Facility”, ERDC/CHL CHETN – II-46, U.S. Army Engineer Research and Development Center, Vicksburg, MS

Wiegel, R. L., (1962), “Diffraction of Waves by Semi-infinite Breakwater,” Journal of the Hydraulics Division, ASCE, Vol.88, No.HY1, pg.27-44

Wright, L.D., Short, A.D., (1984), “Morphodynamic variability of surf zones and beaches: a synthesis”, Marine Geology, 26, pg.93-118

Yüksel, Y., Çevik, E., Yalçıner, A.C., Güler, I., Arı, H.A., Öztürk, M.N., and Ayat, B., (2004), “Kıyı Çizgisinin Modellenmesi ve Karaburun Örneği”, Proje Bitirme Raporu, Yıldız Teknik Üniversitesi, İstanbul

Zheng, J., and Dean, R.G., (1997), “Numerical models and intercomparisons of beach profile evolution”, Coastal Engineering, Vol30, pg.169-201

APPENDIX A

SEASONAL BASED LONG-TERM PROBABILITY DISTRIBUTIONS FOR SIGNIFICANT DEEP WATER WAVES AT BAFRA DELTA

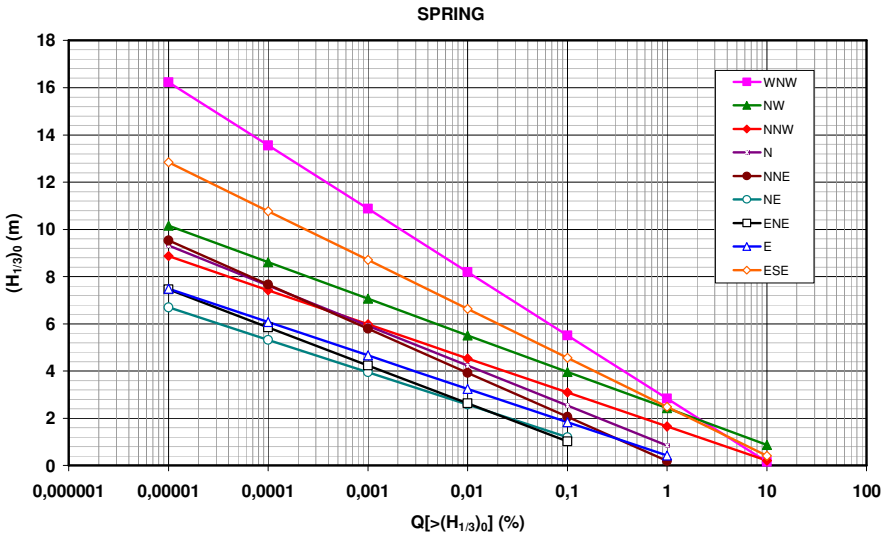

(a)

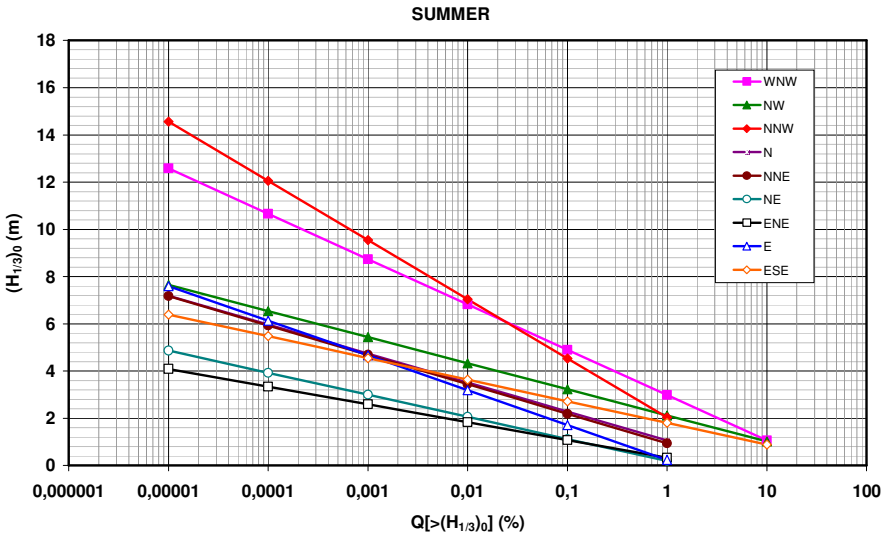

(b)

Figure A.1 Probability distributions of deep water significant wave heights for seasons

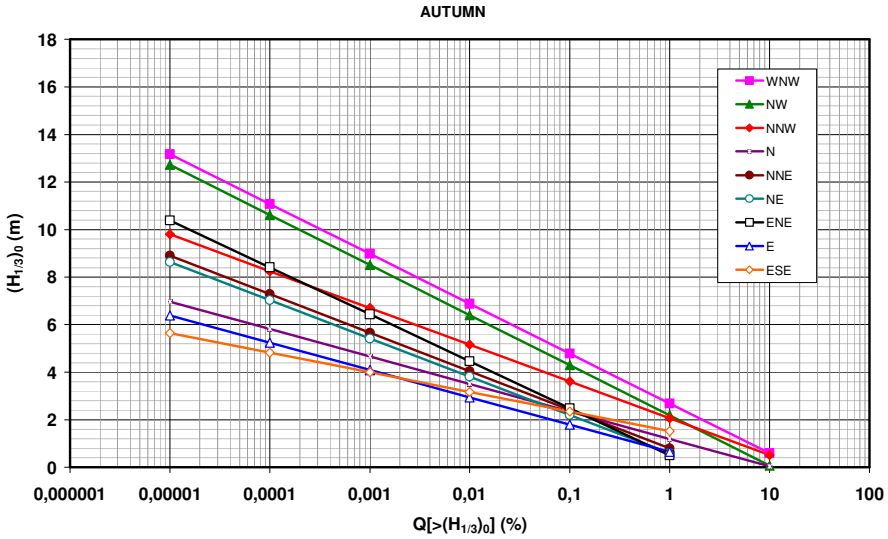

(c)

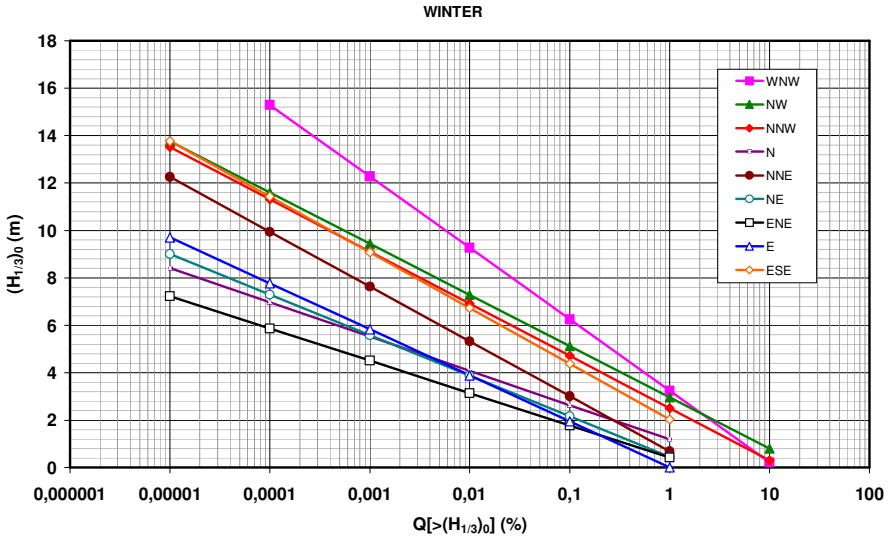

(d)

Figure A.1 Probability distributions of deep water significant wave heights for seasons (cont'd)

APPENDIX B

SAMPLE SIMULATIONS

The execution of the numerical model is introduced for two hypothetical cases; a single groin subjected to uni-directional waves on an initially straight shoreline and a groin field under waves coming from different directions on an initially irregular shoreline.

Simulation 1: A Single Groin

The simplest case to which the numerical model can be applied is a single groin subjected to uni-directional waves on an initially straight shoreline. There are three major inputs for the model; initial shoreline, structural information and wave data (see Figure 3.3). The execution of the numerical model starts with the definition of shoreline position and site specific characteristics. The initial shoreline position may be defined in two different ways; either it can be assumed to be initially straight or it can be defined from a file named as "`kiyi_cizgisi`" that consists of shoreline coordinates in x (alongshore) and y (off-shore) directions. The wave data includes significant deep water wave height (H_0) in meters and corresponding period (T) in seconds, deep water wave approach angle (α_0) in degrees and the frequency (f) in hours and is read from a file named as "`dalga`". The wave data used for this simulation is given in Table B.1.

Table B.1 The wave data input used for Simulation 1

```
1.000 , 4.000 , 30.000 , 1000
```

```
Initial shoreline:
[1]:Initially straight shoreline
[2]:Read from file
1
Enter the length of shoreline in m.:
1000
Initial shoreline coordinate in m.:
0.0
Enter the alonghsore distance increment, dx, in m.:
10
Enter time increment, dt, in hours.
0.5
Enter the median grain size diameter (D50) in m.:
0.0004
Enter beach berm height above still water level:
2.0
...
```

After the initial shoreline position and the wave data input are entered to the program, the structural information is given. For a single groin, the alongshore location of the groin with respect to x=0, the groin length measured from initial shoreline position to the tip of the groin and the permeability coefficient of the groin (Şafak, 2006) are given.

```
Enter the number of sources/sinks:
0
Enter the number of seawalls:
0
Enter the number of tapered beach fills:
0
Enter the number of offshore breakwaters:
0
Enter the number of groins:
1
Enter the distance of groin 1 from left:
500
Enter the length of groin 1:
200
```

```
Enter the permeability of groin 1:
0
Enter the number of repetitions:
1
0.7862
Execute the program with a smaller "dt" value.
```

At the end of the simulation, if the stability condition is not satisfied ($R_s \leq 0.5$), user is asked to run the program again with a new *dt* value smaller enough to satisfy the stability.

```
...
Enter time increment, dt, in hours.
0.25
...
Enter the number of repetitions:
1
0.3931
```

If the stability is satisfied, the program displays the output that consists of initial and computed shoreline positions with structures' illustrations (see Figure B.1).

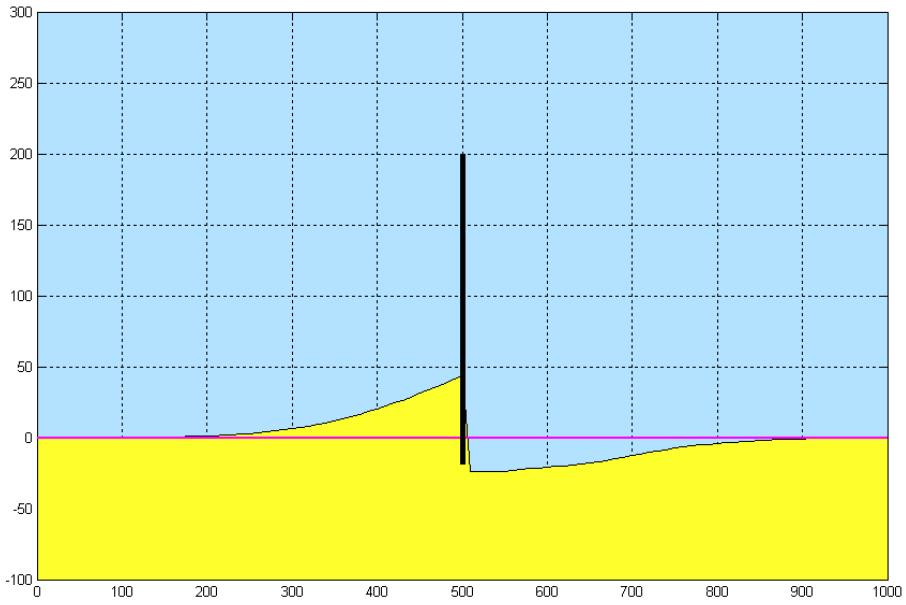

Figure B.1 Final output of the program for Simulation 1

Simulation 2: A Groin Field

In this simulation, the numerical model is applied to a groin field subjected to waves from different directions on an initially irregular shoreline. The initial shoreline position coordinates is read from file (see Table B.2). The numerical model sets the first x coordinate equal to 0 and changes other x coordinates accordingly to make it easy to define locations of the structures with respect to x=0.

Table B.2 The initial shoreline data used for Simulation 2

```
383.1210  , 484.7350
536.7830  , 570.6886
842.0127  , 681.5559
1211.9881 , 746.2285
1655.9586 , 755.4674
2099.9290 , 700.0338
2636.3934 , 616.8833
3228.3540 , 515.2549
3737.0702 , 450.5824
4347.5296 , 413.6266
5031.9841 , 450.5824
5383.1210 , 516.3462
```

The first coordinate value in "*kiyi_cizgisi*" is the x coordinate and the second one separated with a comma is the y coordinate both in meters. The wave data input used is given in Table B.3. The sequence of waves is given with a descending order of deep water wave approach angles herein.

Table B.3 The wave data input used for Simulation 2

```
1.264 , 4.397 ,  67,000 ,  78
1.526 , 4.831 ,  53,886 , 206
0.989 , 3.889 ,  31,386 , 250
1.239 , 4.353 ,   8,886 , 185
1.073 , 4.051 , -13,614 , 135
1.011 , 3.932 , -36,214 ,  58
0.977 , 3.865 , -58,614 , 151
```

```
Initial shoreline:
[1]:Initially straight shoreline
[2]:Read from file
2
Enter the alonghsore distance increment,dx, in m.:
25
Enter time increment, dt, in hours.
0.5
Enter the median grain size diameter (D50) in m.:
0.0004
Enter beach berm height above still water level:
2
Enter the number of sources/sinks:
0
Enter the number of seawalls:
0
Enter the number of tapered beach fills:
0
Enter the number of offshore breakwaters:
0
Enter the number of groins:
5
Enter the distance of groin 1 from left:
1500
Enter the length of groin 1:
200
Enter the permeability of groin 1:
0
Enter the distance of groin 2 from left:
2000
Enter the length of groin 2:
200
Enter the permeability of groin 2:
0
Enter the distance of groin 3 from left:
2500
Enter the length of groin 3:
200
Enter the permeability of groin 3:
0
Enter the distance of groin 4 from left:
3000
Enter the length of groin 4:
200
Enter the permeability of groin 4:
0
Enter the distance of groin 5 from left:
3500
Enter the length of groin 5:
200
Enter the permeability of groin 5:
0
Enter the number of repetitions:
1
0.0830
0.2355
0.1335
0.2637
```

```
0.0819
0.0273
0.0188
```

As the stability conditions for all directions are satisfied, then the resulting output of the program is given in Figure B.2.

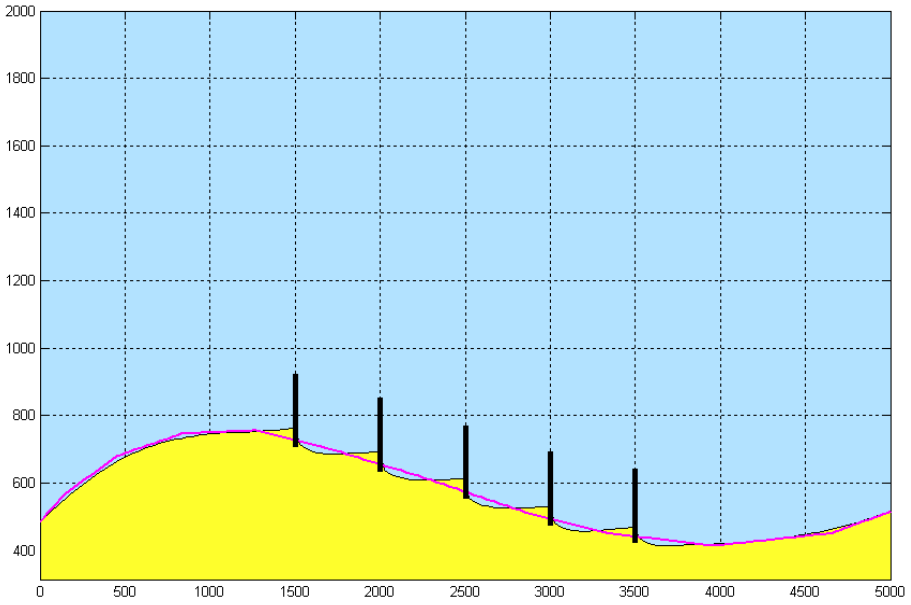

Figure B.2 Final output of the program for Simulation 2